University of Alberta

Shape-Guided Interactive Image Segmentation

by

Hui Wang

A thesis submitted to the Faculty of Graduate Studies and Research
in partial fulfillment of the requirements for the degree of

Doctor of Philosophy

Department of Computing Science

Fall 2012
Edmonton, Alberta

To my beloved family

Abstract

This dissertation contributes to developing shape-guided algorithms for interactive image segmentation. Prior knowledge which describes what is expected in an image is the key to success for many challenging applications. This research takes advantage of prior knowledge in terms of shape priors, which is one of the most common object features, and user interaction, which is a part of many segmentation procedures to correct or bootstrap the method.

In this research, shape-guided algorithms are developed for different types of interactive segmentation: initial segmentation, dealing with certain types of under-segmentation and over-segmentation mistakes, and final object boundary refinement. First, the adaptive shape prior method is developed in the graph cut framework to incorporate shape priors adaptively. After obtaining the initial segmentation, to deal with under-segmentation due to object fusion, the clump splitting method is proposed to take the advantage of shape information on the bottleneck position of the clumps. For over-segmentation which requires merging, the interactive merging method is implemented. Subsequently, to refine the incorrectly segmented object boundaries, the shape PCA method is developed to utilize statistical shape information when intensity information is inadequate. Shape information is embedded as the key in each of the proposed algorithms throughout the whole segmentation process.

To integrate these proposed algorithms together, a comprehensive interactive segmentation system is developed which embeds five decisive tools: addition, deletion, splitting, merging and boundary refinement. By combining these tools, a state-of-the-art shape-guided interactive segmentation system can be constructed which is capable of extracting high quality foreground objects from images effectively and efficiently with minimal amount of user input.

Acknowledgements

I would like to take this opportunity to express my appreciation to those who have helped me through my PhD studies. First of all, I would like to give my deepest gratitude to my supervisor, Professor Hong Zhang, who has initiated the ideas which the research described in this thesis is based on. Hong has been patiently helping me growing, not only my research skills but also critical thinking throughout these years. His guidance, inspiration and encouragement have ensured the success of this research.

I would like to thank Professor Nilanjan Ray, for his guidance and support throughout my PhD studies. I thank my committee members, Professor Martin Jägersand, Professor Scott Acton, and Professor Mrinal Mandal, in spending their time on reading my thesis and providing me feedback on this research. Thanks to Mark Polak and Rajarshi Maiti for providing me a lot of feedback on the segmentation system. I am also very grateful to those in the CIMS lab and Robotics lab at the Department of Computing Science, University of Alberta, who have helped and supported me throughout these years. I would also like to acknowledge the support from all the professors, colleagues and friends whom have taught me, supported me and inspired me throughout the years, directly and indirectly.

Finally, I would like to dedicate this thesis to my beloved parents and my husband Mikael Renström. I deeply thank my parents for their endless love and support for my life and education all these years, as well as their belief in my abilities. Mikael's love and support have made my PhD studies an incredible journey, and he has never stopped being a source of ideas and inspiration for my work. Without my family's love, support and encouragement, this thesis would never have been possible.

Contents

List of Tables

List of Figures

Chapter 1

Introduction

1.1 Problem Motivation and Formulation

In digital image processing, image segmentation is generally an important part of image analysis. Image segmentation refers to the process of subdividing an image into its constituent parts or objects [33]. In other words, image segmentation subdivides an image into different parts at a level depending on the problem to be solved, i.e. the purpose after image segmentation.

Automatic image segmentation is challenging. While it is normally easy and fast for humans to segment objects from an image, it is difficult for computers to perform this task automatically. Some automatic segmentation algorithms have achieved great success in certain applications. However, for applications such as oil sand mining images, medical imaging, etc., where the image quality is limited by acquisition, image level information such as image intensity is usually not enough for any segmentation algorithm to obtain desired segmentation results. Few automatic segmentation algorithms are completely reliable and robust. Figure 1.1 shows an example of oil sand images from oil sand mining industry in (a), its segmentation result from a state-of-the-art automatic segmentation algorithm using deep neural networks [53] in (b) and its desired output in (c). We can see that even with the state-of-the-art automatic segmentation algorithm, the result shown in (b) still contains obvious segmentation mistakes involving over-segmentation, under-segmentation and incorrectly segmented object boundaries. In this dissertation, under-segmentation refers to segmentation mistakes in which the total number of pixels labeled as foreground in the segmentation result is more than the total number of expected foreground pixels in the ground truth image, while over-segmentation refers to segmentation mistakes in which the total number of pixels labeled as foreground in the result is less than the total number of pixels expected as foreground pixels.

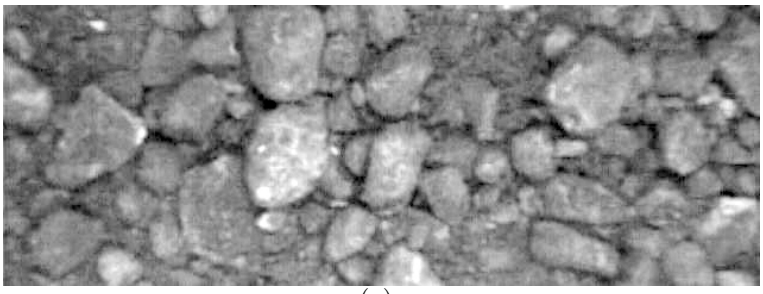

(a)

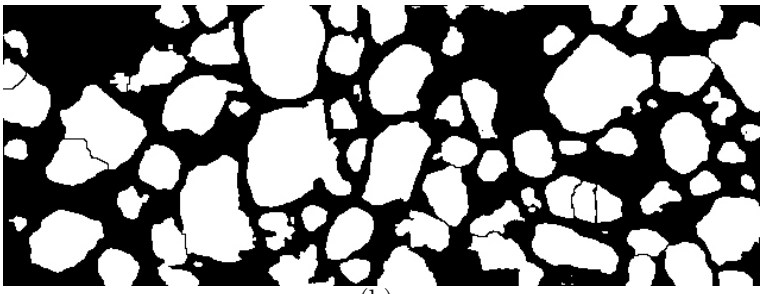

(b)

(c)

Figure 1.1: An example of oil sand images from oil sand mining industry is shown in (a), its segmentation result from a state-of-the-art automatic segmentation algorithm using deep neural networks [53] is shown in (b) and its desired output is shown in (c)

Therefore, image segmentation algorithms should take advantage of prior knowledge to ensure the success in practical and challenging applications. Prior knowledge is discovered to be of great effect on image segmentation algorithms. Prior knowledge describes what is expected in an image. In general, prior knowledge comes in two ways: from human knowledge, such as user interaction at various levels, and from the common properties of the objects of interest, such as shape. User interaction is a part of many segmentation procedures in practice. The interactions are needed to correct or bootstrap an

image segmentation algorithm. In general, an interactive segmentation system can be illustrated in Fig 1.2. In such an interactive segmentation system, the input is typically an image to be segmented. With the help of some prior knowledge, the computational methods generate an initial segmentation of the input image. After that, the user judges the results generated and provides feedback interactively to the system. The system then interprets the user's intention and improves the segmentation accordingly until the user is satisfied with the output. Although there are existing work in interactive segmentation, user interaction can still be very time-consuming and the user's intention may not be correctly interpreted. On the other hand, prior knowledge is available in various image segmentation applications. A segmentation algorithm can make use of prior knowledge such as shape, texture, etc., which are common object features, to obtain what is expected in an image.

The primary focus of this dissertation is therefore, to improve image segmentation by shape-guided algorithms within an interactive segmentation framework which requires minimal user interaction. Shape information which is the key to ensure successful segmentation is embedded in each of the developed segmentation algorithms, throughout the whole segmentation procedure. User interaction is utilized to judge what types of segmentation algorithms are needed, initialize appropriate segmentation positions, choose proper parameters for the algorithms, etc. As subsequent chapters will demonstrate, shape priors and user interaction can be utilized in segmenting challenging images.

1.2 User Interaction in Interactive Image Segmentation

Interactive image segmentation, as opposed to fully automatic one, means the process of partitioning an image into its constituent parts or objects with the help of user interaction. While automatic image segmentation algorithms

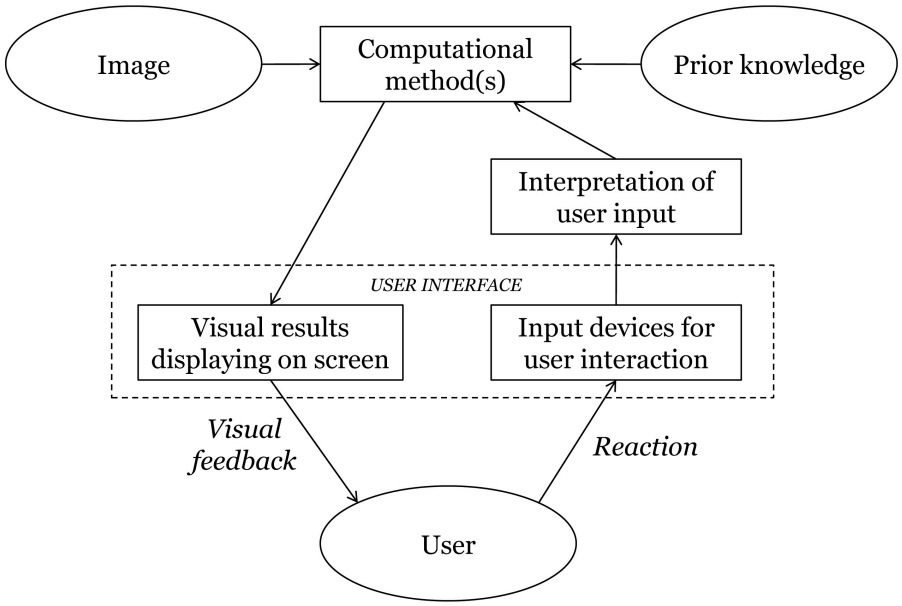

Figure 1.2: The illustration of an interactive image segmentation system, which includes the input image, the user, the computational segmentation algorithm(s) with some prior knowledge, and the user interface.

have been difficult in many applications, interactive image segmentation has become more and more popular. Although some existing work differentiates between *interactive* segmentation and *semi-automatic* segmentation [36] in the way that *interactive* segmentation involves the user in both the initialization and the post-processing stages of the segmentation process iteratively, while *semi-automatic* segmentation only involves the user in the initialization stage, this dissertation unifies these two terms and refers to *interactive* segmentation as any segmentation which requires some kind of user input.

A variety of interactive segmentation algorithms have been proposed in recent decades. In general, different interaction strategies influence the segmentation results in different manners. The success of an interactive segmentation system depends on the combination of the type of user input, how the input is interpreted as the feedback to the segmentation algorithms, and how the feedback is applied in the context of the interactive segmentation process.

In the rest of this section, we will give a comprehensive review of interactive image segmentation algorithms.

1.2.1 Initialization in Interactive Segmentation

The initialization for image segmentation refers to the procedure for setting an initial starting point such as proper segmentation positions on an image, proper values for parameters in the segmentation algorithms, etc. As mentioned, despite the efforts, few fully automatic segmentation algorithms are completely reliable and robust due to noisy image qualities, object occlusions, etc. Therefore, user interaction in the initialization stage is the first and crucial step in deciding the success of a segmentation task.

Initialization interaction can be generally categorized by the way of the user interaction: seeding, such as snake and active contour based methods [42]; labeling foreground and background pixels with strokes, such as the graph cut methods [16, 71] and watershed methods [62]; region of interest, such as bounding box method [50]; boundary tracking and boundary editing, such as livewire [63] and lazy snapping [56]. A combination of these types of interactions also exist in the literature [14, 55, 96, 51, 90, 57].

Although snake and active contour based methods [42] are classic tools in image segmentation, they are sensitive to the positions of the seeds. With seeding followed by energy minimization, they are also not flexible and interactive enough when repeated user editings are required to achieve a satisfying result. Livewire methods [63], on the other hand, allow objects of interest to be extracted via mouse tracings. Although these methods achieve improvement on the accuracy of object boundaries, the amount of human interaction is intensive. More recently, graph cut methods [16, 71, 46] have achieved success, because they not only are efficient and globally optimal, but also allow one to incorporate user interaction easily, such as labeling the background

and foreground pixels with strokes. Besides seeding, specifying foreground or background pixels, etc., more recent interactive segmentation algorithms have incorporated user interactions in the form of combining initialization, boundary editing and boundary tracing [64, 56, 67, 58, 10]. Even though some of these methods claim to be easy in image segmentation and boundary refinement, the amount of user interaction is tedious. Besides, it is easy to lose direct control from the user, i.e., the user's intention cannot always be correctly interpreted in the interaction procedure.

1.2.2 Post-processing in Interactive Segmentation

Besides initialization, post-processing is also a critical step after the segmentation algorithms are performed. Post-processing allows the user to adjust the segmentation results to become more suitable for different purposes, etc. State-of-the-art post-processing techniques include methods such as mathematical morphology, merging small adjacent regions, filtering small objects, filtering badly shaped objects, filling holes, etc. [34, 5, 94, 11] While blindly applying automatic post-processing methods might not achieve desirable results, manually tuning the parameters for a specific application or manually tracing the boundary of the desired object is time-consuming and not generally applicable.

In the literature, Olabarriaga [66] has proposed a human computer interactive framework to tackle the segmentation of medical images with human interaction in the post-processing steps. This framework makes strong assumptions that the user is capable of identifying the needs for post-processing and providing the proposed computational methods prompt feedback to correct the result. However, they apply similar computational methods for all post-processing cases, which are not generally applicable. Sarigul [75] has presented a system for refinement and analysis of segmented CT/MRI images. In

their system, a post-processing method is proposed and applied to CT/MRI images. The system is developed based on rules such as region property, size, etc. Although the system claims to observe the human interaction and apply corresponding automated techniques to develop its own refinement rules, the post-processing operations proposed are insufficient for segmentation mistakes.

1.2.3 Summary

In summary, most existing research on interactive image segmentation involves user interaction in either the initialization, boundary editing/tracing or post-processing steps. While user initializations are not sufficient to generate desirable results on challenging images, algorithms with boundary tracing are very time-consuming. Although some post-processing methods have been proposed to tackle mistakes made by existing segmentation algorithms, these proposed methods are sometimes unable to interpret the user's intention correctly, insufficient and not generally applicable.

This motivates the research of this dissertation to developed an interactive image segmentation system which both reduce the amount of user interaction and better interprets the user's intention. Based on the observations that there are a finite number of segmentation mistakes from existing segmentation algorithms and most mistakes are still confined to part of the desired object of interest, we will propose an interactive segmentation framework by the types of mistakes made by existing segmentation algorithms. We will conclude that there are commonly five types of mistakes made by any segmentation algorithms. Subsequently, five types of interactive tools are needed to deal with each of the failure cases. The overall goal is to take advantage of minimal amount of user interaction which can be correctly interpreted for the user's intention, to benefit interactive image segmentation. The details of this system will be presented in Chapter 5.

1.3 Shape Priors in Image Segmentation

After obtaining different types of user interaction, corresponding segmentation algorithms are needed to perform the segmentation tasks. While some segmentation algorithms tend to analyze images by using pure low level information such as edge information, some other strategies tend to use prior knowledge about what is expected to be segmented from the image. Such prior knowledge usually reflects the common properties of the desired objects. Shape priors are one of the most obvious and important common features in a big amount of image analysis task. Therefore, the second focus of this dissertation is to develop shape-guided segmentation algorithms for different types of interactive image segmentation. In the following section, we will present some reviews on existing shape-guided segmentation algorithms based on the types and purposes of interactive segmentation, i.e., generating the segmentation with shape priors, solving certain types of under-segmentation issues caused by object fusion by clump splitting, and refining final object boundary.

1.3.1 Shape Priors in Graph Cut

Shape priors have been incorporated in various ways in image segmentation. If an object of a certain shape is expected as the output of a segmentation algorithm, a shape constraint can be imposed on the shape of a foreground object. Most existing popular shape based methods incorporate shape information into a specific image segmentation algorithm, such as active contour, graph cut, etc. After incorporating shape information, the segmentation problems can then be formulated in terms of energy minimization. Some energy minimization problems can be formulated further to the max-flow/min-cut problem in a graph, which represents one of the most popular and successful interactive segmentation algorithms: graph cut [16].

Shape priors in graph cut have also been developed in a number of ways. The shape prior term is usually defined in the energy function to penalize the discrepancy between the segmented shape and the expected shape. Some methods express this shape prior term using a shape template [101, 61, 32, 47], while others regulate it as a more flexible constraint [85, 25]. These shape priors have made graph cut segmentation even more successful in challenging data sets.

However, one of the issues with shape prior methods is the selection of the weight on the shape term in the energy function. The weight is usually tuned beforehand to achieve the best result for a certain type of images. Several existing works have mentioned the need to adjust the weight on the shape term depending on the type of images. Even within the same type of images, the needs of a shape prior at different pixels might vary significantly due to noise and intensity inhomogeneities. Therefore, setting a constant weight for the shape prior for all pixels on the whole image is not appropriate. This leads to our proposed adaptive shape prior (ASP) method, which combines image intensity information and shape information adaptively, based on the different needs for the shape prior at different locations of the image. The details on the ASP method will be described in Chapter 2.

1.3.2 Shape Priors in Clump Splitting

When performing segmentation of an image, multiple objects of interest can cluster into clumps. Especially for images with heavily touching or overlapping objects, such cases could seriously affect the overall success of the image analysis task. Existing clump splitting methods can be generally categorized into morphological methods [33, 35, 60, 72, 83], watershed methods [13], model based approaches [39, 6, 59], and concavity based analysis [97, 92]. Almost all the methods in the literature assume binary images, discard the original

intensity information and only work on object shape by, for example, finding dominant or concavity points on the boundary of the binary segmentation.

Although concavity analysis offers an intuitive way of splitting and is so far the most popular technique in clump splitting, the procedure of finding the splitting points and split lines is very parameter-dependent. Concavity based methods also suffer from other limitation mentioned in Chapter 3. Therefore, we will present a novel clump splitting method via bottleneck detection, which takes advantage of the bottleneck positions on the clumps effectively and overcomes the drawbacks mentioned above. The details on this method will be described in Chapter 3.

1.3.3 Shape Priors in Boundary Refinement

At the final stage of the segmentation task, shape priors are also vital parts in refining the boundary of the incorrectly segmented objects. Especially when intensity information is weak or missing, statistical shape information plays an important role. Statistical shape analysis describes the geometrical properties statistically from a set of similar shapes. In the last two decades, model-based segmentation has been successful in shape based image analysis. By matching a statistical model which contains shape information about the expected shape in an image, the segmentation algorithm can perform image segmentation effectively.

One of the problems with current statistical shape models is that when intensity information is very inadequate or missing, statistical models developed from statistical shape analysis such as active shape model have difficulties converging to the correct segmentation. Therefore, we focus on improving the segmentation boundary when image intensity information is inadequate or missing. In Chapter 4 we will describe the proposed shape PCA method, which works by taking advantage of statistical shape information only, which

is not directly available from the image, to improve image segmentation in boundary refinement.

1.4 Contributions

This dissertation introduces novel shape-guided algorithms for interactive image segmentation. We propose three shape-guided algorithms for different stages of the segmentation process: initial segmentation, clump splitting and boundary refinement. To integrate these shape-guided algorithms, a comprehensive interactive segmentation system is developed which efficiently incorporates user interaction. Specifically, the user interaction takes place in a scenario where the segmentation results are progressively refined by a combination of these shape-guided methods. The major contributions of this Ph.D. thesis are:

- **Adaptive shape prior (ASP) method.** An adaptive shape prior method is proposed for incorporating shape priors into the graph cut based segmentation framework to eliminate incorrect cases in previous approaches in which the parameters for the shape prior have to be tuned to fit the image. The adaptive shape prior works by adding the shape term in the energy function based on a probability map, which is straightforward to calculate and does not add much additional cost to the algorithm. With the help of the probability map which can be utilized to reflect the different needs of the shape prior at different locations of the image, the ASP method combines information from both image intensity and shape level adaptively. The ASP method can be easily applied to various types of graph cut segmentation algorithms with shape priors, such as Freedman *et al.*'s graph cut method, and star shape prior method.

- **Clump splitting method via bottleneck detection.** The clump splitting method solves a very common and critical type of segmentation mistake: under-segmentation due to object fusions. In most existing clump splitting methods, the objects to be split into are expected to have roughly convex shape. The proposed clump splitting method therefore focuses on clumps with their splitting points occurring at bottleneck positions of the binary clump. It aims at finding splitting points via bottleneck detection, and obtaining a cutting line with the help of finding connected pixels between splitting points which minimize an energy function. To help with multiple splitting cases, a shape classification based method is also proposed to decide whether to split a connected component iteratively.

- **Shape PCA method.** In order to refine the boundary of the incorrectly segmented objects in the final stage of the image segmentation task, the shape PCA method takes advantage of statistical shape level information, which is not directly available from image level, and refines the shape of the incorrectly segmented object with the first few principal components, which presumably represent the true shape of the object. The local Shape PCA method is also proposed to compare with the global shape PCA method. As long as the incorrectly segmented portions of the object boundary can be localized correctly, either automatically or manually, local shape PCA can be easily applied to perform boundary refinement.

- **A shape-guided interactive segmentation system.** To integrate all of the shape-guided algorithms proposed in this dissertation together with minimal user input, a novel comprehensive shape-guided interactive segmentation system is developed. The proposed system includes

five decisive tools which intuitively reflect user's intention: object addition, object deletion, clump splitting, object merging, and boundary refinement. These five decisive tools are developed based on common cases of failure from any segmentation algorithms. From observation, most image segmentation tasks can be handled by one or a combination of these five tools. By combining all the shape-guided algorithms proposed in this dissertation, this interactive segmentation system can be constructed into a highly effective and efficient interactive object segmentation system with minimal user input.

1.5 Dissertation Organization

This dissertation is organized as follows. Chapter 2 first reviews different shape priors in graph cut image segmentation, followed by the description of the adaptive shape prior method, which is the first contribution of this thesis. Clump splitting in image segmentation is reviewed in Chapter 3 followed by the description on the proposed splitting method via bottleneck detection. Chapter 4 presents the background on statistical shape analysis, followed by the third contribution of this dissertation, namely the shape PCA method. Chapter 5 describes the comprehensive interactive image segmentation system we proposed in order to integrate all of the proposed shape-guided algorithms, followed by detailed experimental results. Finally, conclusions and future work are presented in Chapter 6.

Chapter 2

Image Segmentation via Adaptive Shape Prior

This chapter presents the first contribution of this dissertation, namely the adaptive shape prior (ASP) method. The adaptive shape prior method combines information from both image level and shape level adaptively, based on the different needs of a shape prior at different locations of the image. This chapter will first review some background on graph cut and shape priors in graph cut segmentation. The ASP method will then be described in details with experimental results demonstrating its effectiveness.

2.1 Introduction

Image segmentation has always been an important and challenging task in computer vision. Since Boykov and Jolly [16] introduced the application of the graph cut algorithm into image segmentation, graph cut has become one of the leading approaches in image segmentation in the last decade, because it not only allows one to incorporate user interaction, but also is an efficient algorithm.

More recently, in order to handle noisy images or images with object occlusions effectively, new methods have been developed in the graph cut segmentation framework to exploit shape priors. Freedman and Zhang proposed to incorporate shape priors in graph cut segmentation by matching the segmented curve with a shape template [32]. Veksler has showed how to implement a shape prior for objects defined as star shaped [85]. Das *et al.* presented a similar idea to incorporate shape priors for shapes defined as compact [25]. In addition, some research activities focus on one or two particular types of objects with particular shapes [79, 47], some on incorporating multiple shape priors into one image [86], and yet some on shape representation and general shape constraints [24, 50].

One of the problematic issues of the graph cut framework is the selection of weights on the various terms in the energy function. These weights are

usually tuned beforehand by the developer of the algorithm to achieve the best result for a certain type of images [69]. For example, Peng and Veksler [69] designed a parameter selection method by measuring segmentation quality based on different features of the segmentation. They ran graph cut for different parameter values and chose the parameters which produced segmentation of the highest quality. However, their method only targets issues of selecting the parameters between the data term and the boundary term in the energy function, while setting a constant weight on the shape prior. For images corrupted by significant noise and intensity inhomogeneities, the needs for a shape prior at different pixels are different in general. Therefore, setting a constant weight on the shape prior term for all pixels may not be appropriate. As an example, columns (b) to (d) in Figure 2.3 and 2.4 on page 32 show examples where different parameter settings for the shape prior can lead to very different segmentation results.

To solve the issue described above, we propose to impose shape constraints selectively, by applying the shape prior adaptively in graph cut. To determine the need for the shape prior at each pixel, we derive a shape weight term based on image intensity. The intuition behind this is that if a pair of neighboring pixels appear similar, there should be a higher weight for the shape constraint in the energy function to compensate for the weak or missing edge information. In this way our method gives flexibility in applying a shape prior, and helps obtaining a segmentation result that better matches with the shape prior. As will be seen in this chapter, this weight on the shape constraint can be easily calculated without much additional computational cost.

Song *et al.* [80] proposed an adaptive framework for segmentation of brain tumors in MRI images within an iterative scheme. They incorporated a shape atlas of probabilistic priors into the graph cut energy function by combining it with the image intensity distribution. However, the "adaptive" idea focuses

on the data term D in (2.1) only [80]. Furthermore, the performance of their method relies a lot on the accuracy of the atlas, and several parameters, such as the weight λ between the data and boundary terms, as well as the scale σ for calculating the neighborhood links [80].

In another study, Bar-Yosef *et al.* [9] proposed a variational method for model based segmentation with an adaptive shape prior, with the help of a shape confidence map. Their prior confidence map was defined to select a shape model among many shape models, with the maximum confidence at each pixel to reflect the reliability of the shape prior at each pixel. The prior confidence map then determines if the segmentation algorithm should follow the shape prior or not at each pixel location. However, their method only focuses on the variational framework with many shape prior models, and has only been applied in one specific application.

In contrast to the previous work, our proposed method tackles adaptive shape prior from a different angle. The weight on the shape constraint is obtained from the available image level information, and it reflects how much each pixel needs the shape prior to help with image segmentation. In other words, we measure the need for the shape prior between a pair of pixels, instead of the reliability of the shape prior.

This chapter is organized as follows. In Section 2.2 we present the background on the graph cut segmentation with shape priors in a unified way to combine the boundary and shape term in the energy function. Then we first describe the issue of parameter selection on the relative importance of each term in graph cut, then present our proposed method for adaptive shape priors and give examples of applying it in some existing graph cut methods with shape priors. Finally we provide the experimental results to demonstrate the generality and superior performance of our approach.

2.2 Graph Cut Image Segmentation

This section presents the background on the graph cut segmentation with shape priors. We will first explain the background on graph cut in terms of graph theory and the max-flow/min-cut optimization. Then the application of graph cut algorithm with shape priors on image segmentation will be presented in a unified way to combine the boundary and shape term in the energy function.

2.2.1 Graph Cut

Many segmentation problems can be formulated in terms of energy minimization. Such energy minimization problems can be further formulated into a maximum flow problem in a graph. Under most formulations of such problems, the minimum energy solution corresponds to the maximum a posteriori estimate of a solution. The term "graph cut" is applied specifically to those models which employ a max-flow/min-cut optimization.

Let $G = \langle V, \mathcal{E} \rangle$ be a weighted graph where V is the set of vertices and $\mathcal{E}$ represents the set of edges. V has two distinguished vertices called a source and a sink. A cut $C \subset \mathcal{E}$ is a set of edges such that the terminals are separated in the induced graph $G(C) = \langle V, \mathcal{E} - C \rangle$. In addition, no proper subset of C separates the terminals in $G(C)$. The cost of the cut C thus equals the sum of its edge weights.

The min-cut problem focuses on finding the cut with minimum cost. According to [46], this can be solved by computing the maximum flow between the terminals (source and sink). The worst case complexity is low-order polynomial, although the running time in practice for the graphs is nearly linear [84].

Figure 2.1 demonstrate an example of such a graph. In Figure 2.1, the

two circles represent the two terminal vertices (source and sink). The squares donate all the other vertices. The *thick red* edges link each terminal to the other vertices, and the *thin black* edges join the non-terminal vertices. The *green dashed* lines represent a cut found which separates the vertices into two sets. The total cost of this cut equals the sum of all the edge weights on all the *black dashed* edges.

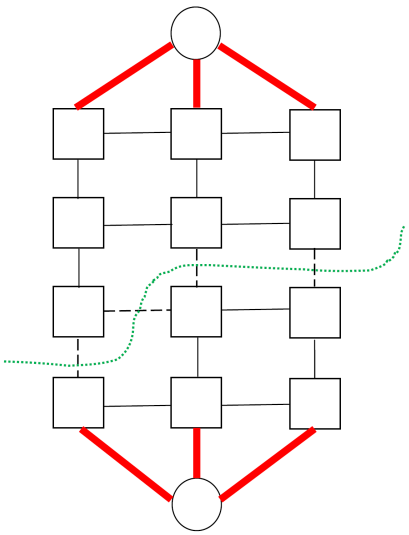

Figure 2.1: Example of graph cut on a graph. In this graph, the two circles represent the two terminal vertices (source and sink). The squares donate all the other vertices. The *thick red* edges link each terminal to the other vertices, and the *thin black* edges join the non-terminal vertices. The *green dashed* lines represent a cut found which separates the vertices into two sets. The total cost of this cut equals the sum of all the edge weights on all the *black dashed* edges.

2.2.2 Graph Cut Energy Function

Graph cut segmentation achieves an optimal solution by minimizing such an energy function via the max-flow/min-cut algorithm:

$$E(F) = \mu D(F) + B(F) \tag{2.1}$$

where $F = (f_1, \ldots, f_p, \ldots, f_n)$ represents a binary vector whose component f_p specifies the assignment of background or foreground to pixel p in an arbitrary set of data elements P in an image I. The data term D represents the cost of labeling F according to the image level information, and the boundary term B denotes the cost of labeling F according to same prior knowledge, such as discontinuity on the boundary. μ is a non-negative coefficient which specifies a relative importance between the boundary term B and the data term D [16]. To be more specific, (2.1) is usually written as:

$$E = \mu \sum_{p \in P} D_p(f_p) + \sum_{\{p,q\} \in N : f_p \neq f_q} B_{pq}(f_p, f_q) \tag{2.2}$$

where N is the set of neighboring pixels on the image I, and f_p represents the label assigned to pixel p. The particular forms for $D_p(f_p)$ and $B_{pq}(f_p, f_q)$ are discussed in the following sections.

2.2.3 Region Term

The region term D_p assumes that the penalties for assigning pixel p to "foreground" or "background" are given. One example of defining the region term D_p is to apply the negative log-likelihood model, which is originally motivated by the MAP-Markov Random Field formulation [16].

$$D_p(\text{“}obj\text{”}) = -\ln Pr(I_p | \text{“}obj\text{”}) \tag{2.3}$$

$$D_p(\text{“}bkg\text{”}) = -\ln Pr(I_p | \text{“}bkg\text{”}) \tag{2.4}$$

where "*obj*" and "*bkg*" represent object and background respectively.

2.2.4 Boundary Term

In graph cut, the boundary term B_{pq} is a penalty term for the discontinuity between a pixel pair p and q. For graph cut without shape priors, $B_{pq} = V_{pq}$.

One example of defining V_{pq} is to penalize the neighboring pixel pairs with high intensity contrast:

$$V_{pq} = e^{(-\frac{(I_p - I_q)^2}{2\sigma^2})} \cdot \frac{1}{dist(p,q)} \tag{2.5}$$

where I_p represents the image intensity of pixel p, σ is a constant and $dist(p,q)$ is usually calculated as the Euclidean distance between pixels p and q [16].

2.2.5 Shape Priors in Graph Cut

If an object of a certain shape is expected as the output of a segmentation algorithm, a shape prior can be used to impose a constraint on the shape of the foreground region. A number of graph cut methods incorporate shape priors by modifying the pairwise term B in the following way:

$$B_{pq} = V_{pq} + \lambda V_{pq}^{'} \tag{2.6}$$

where $V_{pq}^{'}$ represents the newly added shape prior term, and λ is a constant which measures the relative importance of the shape constraint. $V_{pq}^{'}$ is defined in various ways depending on the type of the shape prior, to penalize the discrepancy between the segmented shape and the expected shape.

Some methods express shape constraint using a shape template such as an ellipse [101, 61], while other irregular shape templates are also possible [32, 47]. More recently, the shape constraints in terms of a class of shapes such as the star shape [85] and compact shape [25] have also been proposed. These shape priors are more general and flexible than a single shape template. In all cases, a shape prior needs to be chosen in such a way that is possible to be expressed in a graph representable form. Some specific forms of $V_{pq}^{'}$ in two existing methods will be discussed in the next section.

2.3 Adaptive Shape Prior in Graph Cut

In this section, we will first describe the issue of parameter selection on the relative importance of each term in the energy function of graph cut, present our proposed method for applying a shape prior adaptively, and then we will show how we can apply our method in two existing graph cut algorithms that use a shape prior.

2.3.1 Parameter Selection for Shape Priors in Graph Cut

One of the outstanding issues of the graph cut framework is the selection of weights on various terms in the energy function. These weights are usually tuned beforehand by the developer of the algorithm to achieve the best result for a certain type of images [69]. Several papers on graph cut with shape priors have mentioned the need for a user to adjust λ depending on the type of image. However, for images with spatially varying quality, the needs of a shape prior at different pixels might vary significantly. In other words, setting a constant value λ in (2.6) for all pixels on the whole image is not appropriate. Again, we refer to Figure 2.3 and 2.4 on page 32 to demonstrate the sensitivity of the segmentation result to the choice of λ.

As mentioned, Peng and Veksler [69] studied a parameter selection method for μ in (2.1) by measuring segmentation quality. Further to the selection of μ, our proposed method solves the problem of choosing λ in (2.6) on the shape constraint $V_{pq}^{'}$ adaptively on a per pixel basis. In other words, our method uses a spatially varying weight on the shape prior.

2.3.2 Adaptive Shape Prior

Based on our discussion in the previous section, we propose to incorporate a shape prior adaptively, according to the needs of the shape prior at different

pixels. Specifically, we notice that the pairwise term in (2.6) can be modified in the following way that replaces the constant λ with an adaptive weight S_{pq}:

$$B_{pq} = V_{pq} + S_{pq}V'_{pq}. \tag{2.7}$$

The weight S_{pq} can be estimated from either the original image or an enhanced version of it that we refer to as probability map A, which will be discussed further in the next section. Intuitively, the addition of S_{pq} allows us to impose a stronger shape prior term at locations where the edge information is weaker or less obvious, and vice versa.

The shape weight S_{pq} can be defined in various ways. The higher the similarity is between pixels p and q, the less information there is in the image to allow graph cut to find the boundary of the object, and the stronger the shape constraint should be to help a graph cut algorithm.

First, we introduce a probability map A which has the same size as the image to be segmented. We let α_p denotes the likelihood of a pixel p in the image belonging to the foreground. The value of α_p should be between 0 and 1. Then we define S_{pq} in terms of the A map. To reflect the difference on the probability value of pixels p and q, we use $S_{pq} = e^{-(\alpha_p - \alpha_q)^2}$ in our experiments.

2.3.3 Probability Map A

Various methods exist to compute the probability map A which reflects the likelihood of each pixel belonging to the foreground object. For example, A could be obtained from unsupervised matting [2, 51, 52]. As an alternative, A can also be obtained from supervised learning techniques [41]. In fact, in the simplest case, A can be a smooth or denoised version of the original image.

In our experiments, we will show image segmentation results from two different types of A map, one from denoised images, and one from an unsupervised matting method [51, 52]. Since the focus of this thesis is not to compare

the performance of unsupervised and supervised methods for computing A, we only discuss experiments that use unsupervised methods. In our experiments, the denoised images are generated by applying a Gaussian filter on the original images, and matting images are generated from an existing matting method [51, 52].

Examples of the original images and their enhanced versions serving as the probability maps are shown in Figure 2.2. The first row shows the original images, and the second and third rows show the corresponding probability maps by denoising and matting [52]. To demonstrate the generality of our method, our experiments include images in four different application domains: (a) ore images in mining, (b) shovel tooth images from an excavation shovel, (c) bladder images in medical applications and (d) star fish images.

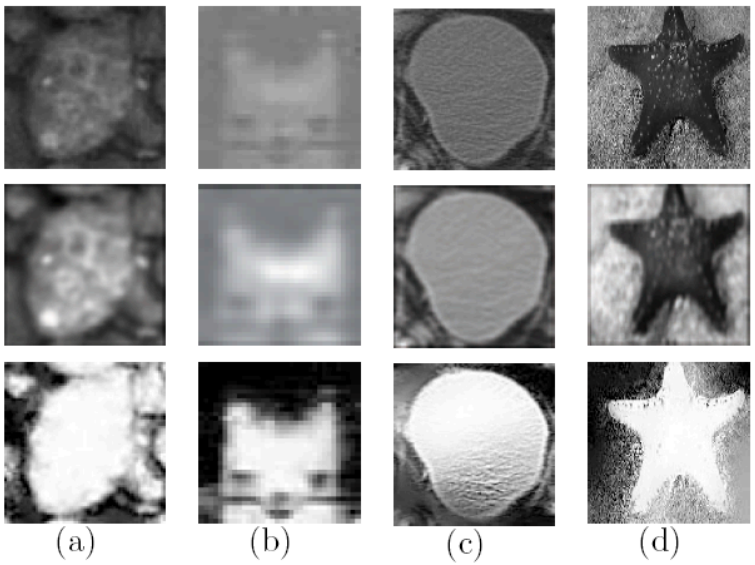

Figure 2.2: Examples of test images and their corresponding probability maps A. From (a) to (d), the images are ore fragment image, bladder image, star fish image and image of an excavation shovel tooth. The top row shows the original images, the middle row shows the corresponding probability maps from denoised images, while the bottom row shows the corresponding probability maps from an unsupervised matting method [52].

2.3.4 Adaptive Shape Template Method

Freedman and Zhang introduced the idea of incorporating a shape template in the form of level set to graph cut [32]. Their method begins with the assumption that the shape prior is a single fixed template [32]. In order to incorporate the shape prior, they modified the original energy function of graph cut by the shape term in Equation (2.6) as:

$$V_{pq}^{'} = \bar{\phi}\left(\frac{p+q}{2}\right) \tag{2.8}$$

where $\bar{\phi}$ is a regular unsigned distance function whose zero level set corresponds to the shape template curve $\bar{c}$. By adding this shape energy term $V_{pq}^{'}$, minimization of the graph cut energy function encourages the object boundary to be aligned with the zero level set [32].

To be more detailed, after adding the shape energy term $V_{pq}^{'}$, the energy function for Freeman and Zhang's shape template method can be written as:

$$\begin{aligned} E(f) = \quad & \mu \sum_{p \in P} D_p(f_p) + \sum_{(p,q) \in N: f_p \neq f_q} V_{pq}(f_p, f_q) + \\ & \lambda \sum_{\{p,q\} \in N: f_p \neq f_q} \bar{\phi}\left(\tfrac{p+q}{2}\right). \end{aligned} \tag{2.9}$$

A drawback of Freeman and Zhang's method is the requirement of object-template alignment through a variety of transformations which are computationally expensive. Another more relevant limitation is the difficulty in choosing a proper λ, which is a common problem for existing graph cut methods with shape priors.

Following our proposed adaptive shape prior pairwise term in (2.7), we can redefine the pairwise term in the energy function (2.9) to be adaptive as in (2.7). That is, the energy function (2.9) for Freedman and Zhang's method can be redefined as:

$$\begin{aligned} E(f) = \quad & \mu \sum_{p \in P} D_p(f_p) + \sum_{(p,q) \in N: f_p \neq f_q} V_{pq}(f_p, f_q) + \\ & \sum_{\{p,q\} \in N: f_p \neq f_q} S_{pq} \bar{\phi}\left(\tfrac{p+q}{2}\right). \end{aligned} \tag{2.10}$$

2.3.5 Adaptive Star Shape Method

A more recent graph cut method with a generic shape prior is the star shape prior method [85]. The star shape prior is not specific to any particular shape, but rather defines a class of shapes. With the assumption that a center of the object is known, the star shape prior method adds a shape constraint to the graph cut energy function as described below.

Consider a center of the star shape is denoted as c. Let 1 and 0 be the object label and the background label, respectively. For an object to be a star shape, for any point p inside the object, every single point q on a straight line connecting c and p must also be inside the object. This implies that if p is assigned label 1, then every point between point c and p is also assigned 1. With the assumption that q is between c and p, the star shape method defines the following pairwise shape constraint term $V_{pq}^{'}$:

$$V_{pq}^{'}(f_p, f_q) = \begin{cases} 0 & \text{if } f_p = f_q, \\ \infty & \text{if } f_p = 1 \text{ and } f_q = 0, \\ \beta & \text{if } f_p = 0 \text{ and } f_q = 1 \end{cases} \tag{2.11}$$

where β is a weight constant.

To be more detailed, after adding the shape energy term $V_{pq}^{'}$, the energy function for the star shape method can be written as:

$$\begin{aligned} E(f) = \quad & \mu \sum_{p \in P} D_p(f_p) + \sum_{(p,q) \in N: f_p \neq f_q} V_{pq}(f_p, f_q) + \\ & \lambda \sum_{(p,q) \in N: f_p \neq f_q} V_{pq}^{'}(f_p, f_q) \end{aligned} \tag{2.12}$$

where $V_{pq}^{'}$ is a shape energy term defined by (2.11).

Similar to other shape prior methods in graph cut segmentation, the star shape method still has the limitation with parameter selection for different terms in the energy function. As discussed in [85], β needs to be chosen appropriately by the user in order to obtain good segmentation results. It is obvious that λ and β are relative weights, and the problem of selecting them remains.

Following similar procedure as for the shape template method, we can redefine the pairwise term in the energy function (2.12) to be adaptive as in (2.7). That is, the energy function (2.12) can be redefined as:

$$\begin{aligned} E(f) = \quad & \mu \sum_{p \in P} D_p(f_p) + \sum_{(p,q) \in N: f_p \neq f_q} V_{pq}(f_p, f_q) + \\ & \sum_{(p,q) \in N: f_p \neq f_q} S_{pq} V'_{pq}(f_p, f_q). \end{aligned} \tag{2.13}$$

2.3.6 Optimality of the New Energy Function

A function E is *graph-representable* if there exists a graph $G = (V, \mathcal{E})$ with terminals s and t and a subset of vertices $V_0 \subset V - \{s, t\}$ such that, for any configuration $f_1, \ldots, f_n$, the value of the energy $E(f_1, \ldots, f_n)$ is equal to a constant plus the cost of the mininum cut among all cuts [46]. To be more detailed, if we define the class F^2 energy functions to be written as a sum of functions of up to two binary variables at a time [46], *i.e.*,

$$E(f_1, \ldots, f_n) = \sum_i E_i(f_i) + \sum_{i<j} E_{ij}(f_i, f_j), \tag{2.14}$$

then E is *graph-representable* if and only if each term E_{ij} satisfies the following inequality:

$$E_{ij}(0,0) + E_{ij}(1,1) \leq E_{ij}(0,1) + E_{ij}(1,0). \tag{2.15}$$

Functions which satisfy the condition of (2.15) is called *regular*.

If an energy function E is *graph-representable* by a graph G, it is possible to find the exact minimum of E in polynomial time by computing the min-cut on G [46]. Therefore, as long as an energy function satisfies (2.15), a graph can be constructed and a global optimized solution can be obtained via max-flow/min-cut algorithm.

In (2.10) and (2.13), the V_{pq} term is defined the same as in (2.5). The difference lies in the shape term V'_{pq}. For both (2.10) and (2.13), we have

$V(0,0) = 0$ and $V(1,1) = 0$. As well we have $V^{'}(0,0) = 0$ and $V^{'}(1,1) = 0$. On the other hand, the energy function E is defined to be nonnegative. Therefore $V(0,1) + V(1,0) \geq 0$ and $V^{'}(0,1) + V^{'}(1,0) \geq 0$. Since S_{pq} is nonnegative, and in our experiments β from (2.11) is nonnegative, $S_{pq}V^{'}_{pq}$ is nonnegative as well. This shows that the new energy functions in (2.10) and (2.13) are *graph-representable*. Therefore, we can construct a graph according to [46] and obtain optimized solutions for (2.10) and (2.13) via max-flow/min-cut algorithm.

2.4 Experiments

In order to evaluate the segmentation results from the experiments, different evaluation metrics can be applied. In this section, we will first describe three different evaluation metrics which will be used in this thesis. Some of these metrics will be used for evaluating the results in this chapter, while some others will be used for evaluating results in some other chapters. After describing the evaluation metrics, we will then present the experimental results from our adaptive shape prior method.

2.4.1 Evaluation Metrics

To evaluate the image segmentation performance quantitatively, several evaluation metrics are used in this dissertation. Supervised evaluation is the most widely used evaluation method in image research. It computes the difference between the ground truth and the segmentation result using a given evaluation metric. In this thesis, we apply supervised evaluation methods which compare the segmented results with the ground truth images with three different metrics: **pixel accuracy**, **labeling score** and **Jaccard index**.

For convenience, TP, TN, FP and FN stand for the number of samples (e.g., the number of pixels or the number of objects) being labeled as true

positive, true negative, false positive, and false negative.

Pixel accuracy is defined as

$$\frac{TP + TN}{TP + TN + FP + FN} \tag{2.16}$$

Pixel Accuracy is a pixel level criterion which commonly measures the percentage of correctly labeled pixels.

Labeling score is defined as

$$L = min(S(A, B), S(B, A)) \tag{2.17}$$

with

$$S(A, B) = \sum_{j}^{m} \left[\sum_{i}^{n} \left(\frac{|A_j \cap B_i|}{|A_j \cup B_i|} \quad \frac{B_i}{\bigcup\limits_{|A_j \cap B_i| \neq \emptyset} B_i} \right) \frac{A_j}{\bigcup\limits_{j} A_j} \right] \tag{2.18}$$

where A_j is a connected component in image A and B_i is a connected component in image B. This labeling score is based on [70]. It is a form of local intersection-over-union whereby both errors at the pixel level and object level are penalized. In contrast to pixel accuracy, label score not only takes the pixel labeling error into account, but also penalizes over-segmentation and under-segmentation on the object level.

Jaccard index is defined as

$$\frac{TP}{TP + FP + FN} \tag{2.19}$$

Jaccard index is the ratio of intersection and union of the segmented region and ground truth region.

2.4.2 Experimental Results

To validate our proposed shape prior method, we have run experiments on two graph cut methods with shape priors. We use a MATLAB wrapper with the C++ max-flow code by Boykov and Kolmogorov [45]. When comparing our proposed method to Freedman and Zhang's shape template method [32], the shape template is introduced in the same way, i.e., we assume an aligned template as the shape prior. The aligned shape templates for each image are exactly the same for both Freedman and Zhang's method and our method. As mentioned in [32], the key assumption of Freeman and Zhang's method is that, based on the user input, the shape template can be well aligned with the image using the Procrustes Method [27]. Details on the Procrustes Method are described in the later chapter of this thesis on Page 65. Given the aligned template, the distance function can be easily computed via scaling, as the input to the graph cut energy function. It is also mentioned that the rigid transformation computed via the Procrustes Method will not be extremely accurate [32]; however the algorithm is robust in the situation in which the template is not exactly accurate. When comparing our method to the original star shape prior method [85], we also perform our experiments based on exactly the same user initialization to specify a center of the object to be segmented.

We perform our experiments with two different types of probability map A, one obtained by denoising, and the other by an unsupervised matting method [51, 52]. The denoised images are generated from applying a Gaussian filter on the original images. After obtaining the probability map A, the probability map is combined with the shape prior from either Freedman's method or the star shape prior method, and finally the corresponding energy function is minimized via graph cut.

Figures 2.3 and 2.4 show the comparison results of our adaptive method

to the shape template method [32] and the star shape prior method [85], respectively. In both figures, the original images are shown in column (a), and results obtained by the competing methods are shown in columns (b) to (d) with different values of λ. Our results are shown in columns (e) and (f). The difference is that, the results shown in column (e) uses denoised images as the probability map A, while the results shown in column (f) utilizes matting [52]. Table 2.1 and 2.2 show the statistical results. To evaluate the performance of the algorithms quantitatively, we apply two popular evaluation metrics: Jaccard index [40] and pixel accuracy.

In total, our experiments included 20 oil sand images, 46 tooth images, 15 bladder images and 10 starfish images. The last two columns in the tables demonstrate the superior performance of our method over the competing methods. The highlight columns show the best performance in each row. It is clear that our method obtains better segmentation results most of the time without the need to optimize with regard to λ, while the two competing methods both need to tune the parameter λ.

When comparing columns (e) and (f) in Figure 2.3 and 2.4, we obtain almost the same segmentation results even though we use different techniques for obtaining S_{pq}. This shows that our method is flexible in terms of how A is generated. Since we are not interested in picking the best method for computing A, comparison among various types of A is not further examined in our study.

2.5 Summary

We have proposed an adaptive method for incorporating shape priors into the graph cut based segmentation framework to eliminate incorrect cases in previous approaches in which parameters had to be tuned to fit the image. Adaptive shape prior works by adding the shape term in the energy function

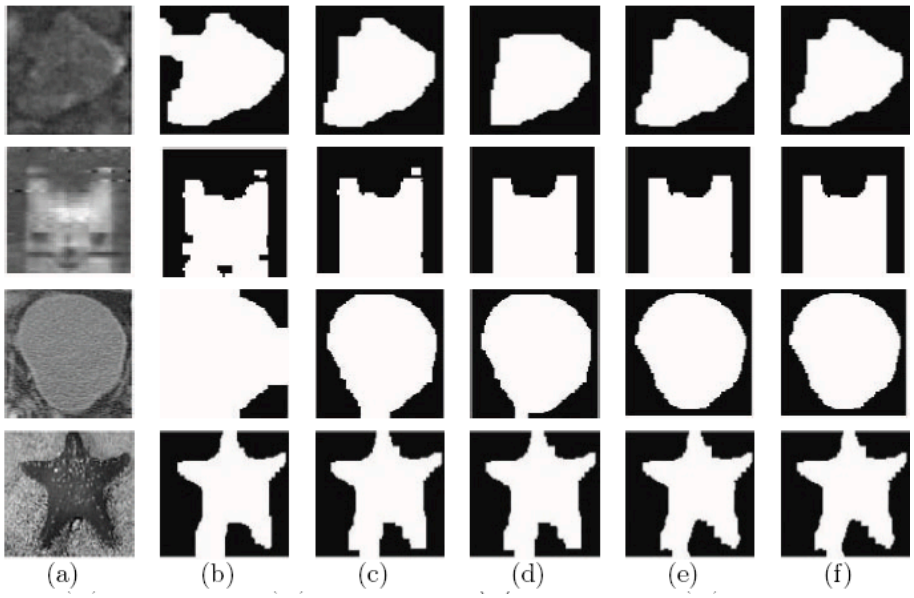

Figure 2.3: Results from Freedman *et al.*'s shape template based method [32]. Column (a) shows the original images. Columns (b)-(d) show segmentation results from Freeman and Zhang's original shape template method with $\lambda =$ 0.2, 0.5 and 0.8. Columns (e) and (f) show segmentation results from our adaptive shape prior applied to Freedman and Zhang's shape prior method. Column (e) uses denoised images as the probability maps A. Column (f) uses matting maps as the probability maps.

Table 2.1: Statistical results comparing Freedman *et al.*'s shape template method [32]. Results with adaptive shape prior method (ASP) by using the denoised images as S_{pq} are shown in the last column. Very similar results were obtained by applying the matting maps as S_{pq}.

Shape Template method		λ=0.2	λ=0.5	λ=0.8	ASP using denoised image as Spq
Oil sand images	Accuracy	0.95	0.97	**0.98**	**0.98**
	Jaccard	0.89	0.95	0.95	**0.96**
Tooth images	Accuracy	0.82	0.86	0.89	**0.92**
	Jaccard	0.81	0.81	0.85	**0.93**
Bladder images	Accuracy	0.83	0.84	**0.85**	**0.85**
	Jaccard	0.78	**0.79**	0.78	**0.79**
Star fish images	Accuracy	0.82	0.83	0.83	**0.84**
	Jaccard	0.77	0.78	0.79	**0.80**

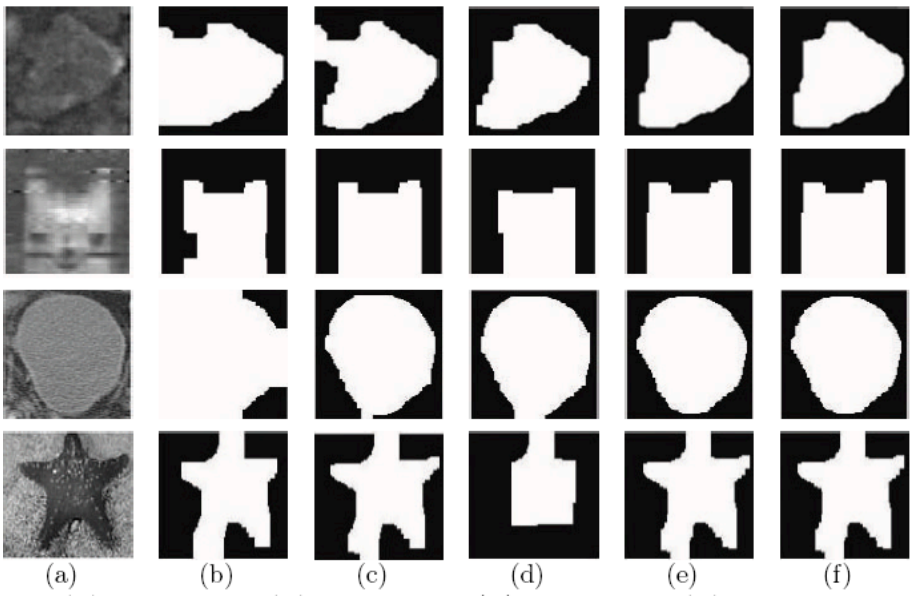

Figure 2.4: Results from the star shape prior method [85]. Column (a) shows the original images. Columns (b)-(d) show segmentation results from the original star shape prior method with $\lambda = 0.2$, 0.5 and 0.8. Columns (e) and (f) show segmentation results from our adaptive shape prior applied to Veksler's star shape prior method. Column (e) uses denoised images as the probability maps A. Column (f) uses matting maps as the probability maps.

Table 2.2: Statistical results comparing the star shape method [85]. Results with adaptive shape prior method (ASP) by using the denoised images as S_{pq} are shown in the last column. Very similar results were obtained by applying the matting maps as S_{pq}.

Star Shape method		λ=0.2	λ=0.5	λ=0.8	ASP using denoised image as Spq
Oil sand images	Accuracy	0.96	0.96	0.96	**0.97**
	Jaccard	**0.92**	**0.92**	**0.92**	**0.92**
Tooth images	Accuracy	0.72	0.81	0.80	**0.91**
	Jaccard	0.55	0.65	0.69	**0.70**
Bladder images	Accuracy	0.84	**0.85**	0.84	**0.85**
	Jaccard	0.78	**0.79**	**0.79**	**0.79**
Star fish images	Accuracy	0.84	**0.87**	0.86	0.86
	Jaccard	0.61	0.62	**0.63**	**0.63**

based on a probability map. We have shown that the proposed method can be easily applied to various types of graph cut based image segmentation algorithms with shape priors, such as Freedman *et al.*'s graph cut method with shape template, and the star shape prior method. Although we need an extra step to obtain the probability map A, this step is straightforward and does not add much additional cost to the graph cut segmentation. In Chapter 5 we will describe how to integrate the ASP method proposed in this Chapter to an interactive segmentation framework.

Chapter 3

Clump Splitting via Bottleneck Detection

In this chapter we will investigate the clump splitting method, which solves a common and critical mistake by existing image segmentation: under-segmentation due to object fusion. Especially, we focus on clumps with their splitting points occurring at bottleneck positions. That is, the objects to be split into are expected to have roughly a convex shape. This is a common case in clump splitting and various clump splitting methods have been developed to deal with this case. This chapter will first present a comprehensive review on existing clump splitting methods, followed by the description of the proposed clump splitting method via bottleneck detection, the second contribution of this dissertation. Experimental results will also be presented to demonstrate the superior performance of this proposed method.

3.1 Introduction

When performing segmentation of an image in different domains, multiple objects of interest tend to cluster into clumps in the image. Generally, clumps are formed due to either touching or overlapping objects, especially when object density is high in the image or if the objects in the image are close to each other. In such cases, clump splitting is required to divide a segmented region into two or more parts or portions. In applications in which the sizes and shapes of the objects in the image need to be accurately determined, the splitting of a clumped object into constituent objects must be performed for optimal segmentation performance. Although a human operator may be able to detect the constituent objects of interest based on prior knowledge, perception of texture and structure of the original image, it still remains a challenge for a computer algorithm to handle this automatically.

Generally, separating clumps using image analysis is not easy. Even in cases where the segmentation of the image between foreground and background is easily achieved because of high contrast between them, the segmentation often

fails to separate the individual objects, which form clumps because of a very high degree of resemblance among the objects in a clump. Therefore, effective and efficient clump splitting methods are needed to resolve under-segmented objects.

3.2 Review of Clump Splitting Methods

Existing clump splitting methods can be categorized into mathematical morphology based methods [33], watershed based techniques [13], model based approaches [39, 6, 59], concavity based analysis [97, 92], etc. Almost all the methods found in the literature assume that the images are binarized and discard the original intensity information [29].

Morphological methods are quite simple and widely used in image analysis tasks. Many of these methods are using basic morphological operations, such as erosion, dilation, opening and closing [35, 60, 72, 83]. However, these methods are generally not accurate when the clumps are heavily clustered. For example, one difficulty with morphology-based methods is that they may completely remove an object of interest in a clump.

Watershed based methods [13] are well known segmentation techniques, which can potentially serve as clump splitting methods. Watershed based methods split a clump based on the intensity surface of the image. For the marker based watershed method, the first step involves the identification of the markers to control the number of objects in the image. Once the markers are obtained, the watershed algorithm is applied with the constraint that the only regional minima are markers. Then the watershed lines obtained are consequently the split lines for the clumps. However, markers are difficult to determine in general. As a result, for objects which vary in size and shape, watershed tends to over-segment the object of interest and, for objects which heavily overlap, watershed tends to under-split them.

Model based techniques are generally popular among some microscopy applications since cells in microscopic images are usually roughly elliptical, and can easily be modeled geometrically. Therefore, template matching and ellipse fitting on the contour of the cells can be effectively applied to cell clump splitting [39, 6, 59, 8]. These methods are in general computationally expensive and parameter-dependent. For example, Liu *et al.* [59] proposed a method for deformable shape based image segmentation by splitting/merging regions in an image. Deformation parameters are optimized by maximizing the agreement of the shapes of the segmented regions with a prior distribution. This method however faces the difficulty in optimization in a high dimensional parameter space. A combination of concavity and model based methods has been presented by Bai *et al.* [8], which proposes a splitting algorithm for osculating cells based on concave points and ellipse fitting. Their algorithm first extracts concave points by using concave property of a region, together with heuristic rules to tackle special cases, such as incomplete cells and non-concave clumps. The algorithm applies ellipse fitting after the contour has been separated by the selected concave points. However, experiments have shown that this concavity based method is only applicable to objects of specific sizes and shapes, and the ellipse fitting procedure is not general to process objects of non-elliptical shapes.

In spite of their limitations, concavity analysis offers an intuitive way of clump splitting. In fact, it is so far the most popular technique in clump splitting. Concavity points refer to the points on the boundary of the clustered objects. With the assumption that such concavity with high curvature is formed due to touching, overlapping, merging of two or more objects, concavity based methods search for dominant concave points. Such methods have been successfully implemented in a variety of application domains [31, 91, 48, 38, 30]. For instance, Fernandez *et al.* used spatial and gradient parameters to

find the lines between concavity points of clumped objects [31]. The method depends heavily on how the split line is defined between each two concavity points. The split line is determined by the threshold values for both the Euclidean distance between the two concavity points and the gradient value for a line to be a candidate line, which is very parameter-dependent. More recently, a rule based method [48] is proposed based on concavity analysis. The method is adaptable to many object shapes and sizes. The concavity analysis depends on a set of parameters which are obtained from a large set of training samples. The procedure of finding split lines is recursive by thresholding on the set of candidate split lines. However, many samples in [48] are synthetic and it is not clear to what extent this method can handle object overlap. The method is also computationally expensive. An improved version of this rule based method has been developed recently by Farhan *et al.* [30]. This improved method modifies [48] by changing the definition of the unit vector. This method also incorporates several key features from [95]. However, it still suffers from the similar disadvantages from [48] that are fundamental limitations in all concavity based methods.

3.3 Drawbacks with Existing Methods

For most concavity and model based methods, identifying candidate points for splitting is the first step to locate where the splits occur on a clump, assuming that the clump to be split has been identified. As has been mentioned, the techniques for determining splitting points in concavity based methods are usually limited to objects of specific sizes and shapes and are sensitive to noise. For instance, the contour of a clump usually has many local concave regions, which make the performance of these concavity based algorithms suffer negatively. Furthermore, to find valid concave points, these methods need proper initial settings of parameters. Thus, these methods are not general enough for

clump splitting. In addition, as will be shown in this study, concavity points are not always the best candidate points for splitting. Although Bai *et al.* [8] proposed an extra step by adding points which are not concave points for splitting, this extra step is not always accurate and efficient, due to its assumption that the objects are similar in both shape and size.

To demonstrate this issue, in Figure 3.1, columns (a) - (d) show four different clumps. The red circles on the contours represent points found for splitting. The first row shows the results from a classical concavity based method, which can only find one concave point, because the second splitting point is not a concave point. The second row shows the results from more recent concavity based methods such as [8] and [48], which can find the second splitting point through some rules. Unfortunately, since these rules normally assume that the size of the two splitting candidates should be almost the same size, the second points found are not necessarily the correct splitting points. The third row show the results of our method based on bottleneck detection, which correctly identifies a pair of splitting points in each of the cases. We will discuss the details of our bottleneck detection method in Section 3.4.2.

To join each pair of selected splitting points, almost all the methods found in the literature assume that the images are binarized and discard the original intensity information [29]. Some splitting algorithms blindly join two selected points with the shortest Euclidean distance. Some other splitting methods apply the short cut rule [78], that is, if boundary points can be joined in more than one way, the short cut rule prefers the shortest cut. However, these methods may yield inaccurate segmentations. For an application where segmentation accuracy is very important, blindly finding the shortest Euclidean cut between the selected split points may not be optimal. From our observation, existing intensity information from the original image could be helpful in obtaining a more accurate boundary than a straight line joining the pair of

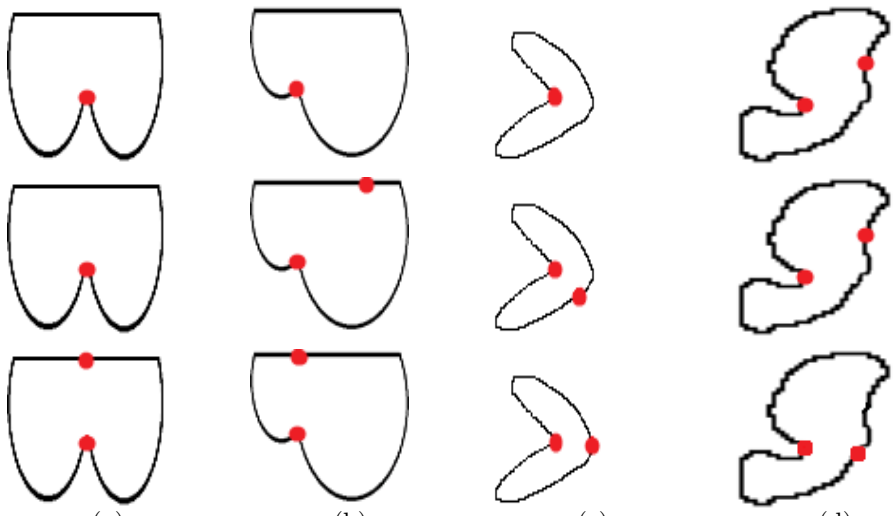

Figure 3.1: Visual comparison on the detection of splitting points. The top, middle and bottom rows show the results from classic concavity based method, which can find only one concavity point; the results from [8] and [48], which are not always the correct points; and the results using our proposed bottleneck detection. The detected splitting points are shown in red circles on the black contour of the clumps.

selected points. We refer to Figure 3.7 on page 55 to demonstrate this issue in our experimental result section.

Another problematic issue with clump splitting is to decide whether a connected component is a clump, and if it is, how many times it needs to be split. While morphology and watershed based methods are parameter-dependent to produce the number of splits, model and concavity based methods generally decide the number of splits at the same time when the candidate split lines are selected. When the best split lines are selected, the number of splits is decided simultaneously. Various methods are proposed for this selection process. For instance, Kumar *et al.* [48] applied a linear SVM classifier to determine the best split line with concavity based features called the measure of split. This classification has significantly improved the results for correct number of splits. Farhan [29] applied Delaunay triangulation to list all candidate split lines, and then made use of saliency, alignment and vector directional features to form a

cost function to select the best split lines. Once the split lines are selected, the number of splits is also determined. However, most of these concavity based methods are quite parameter-dependent in order to set the rules for selecting the best split lines, and they still suffer from the limitation of concavity based splitting methods as we mentioned in the beginning of this section.

3.4 Clump Splitting via Bottleneck Detection

To overcome these drawbacks mentioned in Section 3.3, we propose a novel clump splitting method based on bottleneck detection and shape classification. In contrast to most existing methods which detect splitting points first, and then decide whether to split a connected component at these split points afterwards, in our proposed method, we first decide whether to split a connected component via a shape classification procedure and, if positive, apply the proposed bottleneck detection to split the clump. Admittedly that in an interactive segmentation framework, the decision of whether to split a connected component can be made by the user interactively, we propose such a method through shape classification as an option for the user.

Specifically, our proposed method contains two phases: offline and online. A shape classifier is trained offline and then applied online iteratively. The online phase consists of three steps as summarized by the flowchart in Figure 3.2. For the first step, we apply the shape classifier to decide whether to split a connected component, with the help of a set of shape features. For the second step, we focus on clumps with their splitting points occurring at bottleneck positions. The only assumption made is that the objects to be split into have roughly a convex shape. Based on our survey, this is a common assumption in clump splitting. After locating the bottleneck positions, in the third step, we find an optimal split curve between the selected points, based on minimizing an image energy which corresponds to finding a connecting curve

that visually best splits the constituent objects of interest. Each time a new connected component is generated from splitting, it will go through the shape classification step again until no more splitting is found to be necessary.

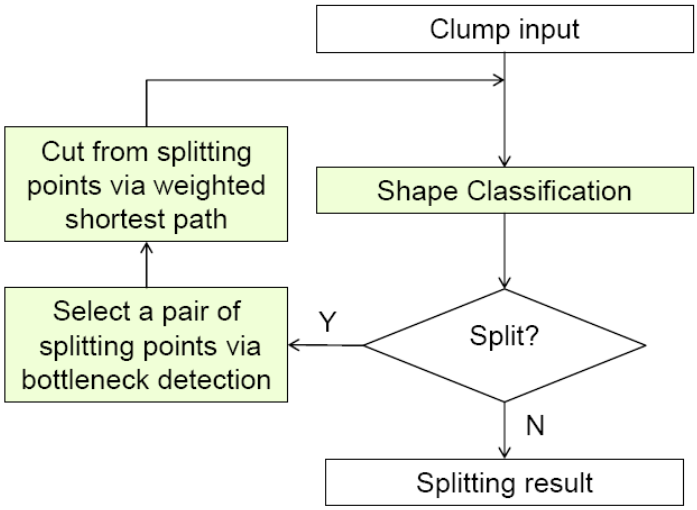

Figure 3.2: Flowchart of the online phase in the proposed clump splitting algorithm.

3.4.1 Shape Classification

This section describes the first step of our proposed method: shape classification. This step is applied at the beginning of each iteration to determine if a connected region should be split. Shape classification is a natural way to determine if a split is necessary [65]. It is our general observation that, shape features such as solidity and convexity are good application-specific features to classify connected regions into splitting and no-splitting cases. Therefore, the input to the shape classifier can be visualized as a matrix having the same number of columns as the shape features we extract. Each row of the matrix corresponds to a connected component. For each application, we build a specific shape classifier based on shape features.

Different learning algorithms can be applied for shape classification based

on shape features. The SVM classifier is used in this study, although other classification techniques are possible. We train the SVM classifier by obtaining the training data from manually selected split and no-split cases. Once trained, the SVM can be used online at each iteration to determine whether to split. We will describe the details of our experiments and demonstrate the effectiveness of our classification for splitting in the experimental result section.

3.4.2 Identify Points for Splitting via Bottleneck Detection

In this section, we will describe the second step of our proposed method: identify a pair of splitting points via bottleneck detection, the vital step on deciding how to split a clump. As mentioned in the literature review, for most concavity and model based methods, identifying candidate points for splitting is performed first. Although various techniques exist in this step, almost all of them suffer from the disadvantage of concavity based methods, such as sensitivity to noise and lack of generality for different object shapes and sizes. We propose to apply the detection of the bottleneck positions for identifying splitting points. For a given clump to split, first we determine where on the contour to divide the clump into two constituent objects. From our observations, the splitting points on a clump should always occur at the bottleneck positions, as a result of the fact that the constituent objects of the clump to be split have roughly a convex shape. Visually, the term bottleneck refers to the narrowest section of a connected component relative to the size of the objects in the clump. Therefore, the bottleneck of a clump is intuitively the most likely place to break and divide the clump.

To find the bottleneck positions, let A and B represent two different points on the contour of a clump. Mathematically, we first define a cost function

between points A and B as:

$$E_s(A,B) = \frac{dist(A,B)}{\min\{length(A,B), length(B,A)\}} \tag{3.1}$$

where $dist(A,B)$ represents the Euclidean distance between points A and B inside the clump, $length(A,B)$ denotes the clockwise length from point A to B on the boundary of the clump, $\min\{length(A,B), length(B,A)\}$ represents the smaller value between the two lengths. Here, we assume that for any clump, the boundary should be one closed curve. Then, we denote by A^* and B^* the positions of the bottleneck on the contour where the cost E_s is minimized:

$$(A^*, B^*) = \arg\min_{A,B} E_s(A,B). \tag{3.2}$$

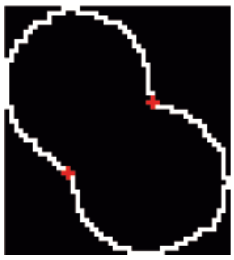

Figure 3.3: Examples of a pair of points found via the bottleneck rule. The red crosses indicate points A^* and B^* located at the bottleneck positions of the white contour.

Figure 3.3 shows a visual example of points A^* and B^* found via (3.2). Again, we refer to Figure 3.1 to show some simple experiments to demonstrate the advantage of the bottleneck method over the traditional concavity point based methods and rule-based methods [48, 8]. We can see that our bottleneck-based method works for situations when points for splitting include non-concave points, or when concave points with very high concavity value are not the optimal candidate locations for splitting. Although [8] and [39] proposed an extra step by adding points which are not concave points for splitting, these extra steps are not always accurate and efficient, as shown in the second row of Figure 3.1.

Even though we only find a pair of splitting points at one bottleneck, our method can be extended easily to finding multiple pairs of points for splitting. We have addressed the determination of the number of constituent objects in a clump in Section 3.4.1 via shape classification. For objects which are classified as split cases via shape classifier, the splitting algorithm will continue to work iteratively via bottleneck detection.

3.4.3 Cut Between Selected Points via Weighted Shortest Path

As mentioned, almost all the methods found in the literature assume that the images are binarized and discard the original intensity information. However, from our observation, intensity information can sometimes be helpful in obtaining a more accurate object boundary. We refer to Figure 3.7 on page 55 to demonstrate this in our experiments. Therefore, we propose to connect the pair of points found in the bottleneck detection step by the weighted shortest path, to be described next. We will also show in the experiments that the proposed method not only makes use of helpful edge information, but also can work in a way similar to the existing methods when edge information is not evident.

To begin with, we crop as the region of interest a small local image patch $\mathbf{I}$ from the original image, around the two selected splitting points A^* and B^*. The size of the image patch $\mathbf{I}$ is defined to be proportional to the object size. Figure 3.4 shows an example on how $\mathbf{I}$ (the highlighted rectangle) is formed, from A^* and B^* found from Figure 3.3. We can see clearly that in this case there exists some useful intensity information which can help in finding the accurate splitting curve.

Intuitively, our goal is to find the strongest edge that connects the two splitting points in the local image patch $\mathbf{I}$. This leads to the following energy

Figure 3.4: Example of the local image patch $\mathbf{I}$ (the rectangle area highlighted). It is determined by the pair of points A^* and B^* found from the previous step.

function based on edge strength:

$$e(\mathbf{I}) = \left(\left| \frac{\partial}{\partial \mathbf{x}} \mathbf{I} \right| + \left| \frac{\partial}{\partial \mathbf{y}} \mathbf{I} \right| \right). \tag{3.3}$$

Given such an energy function, finding a path between points A^* and B^* that maximizes the energy function corresponds to finding a connecting curve that visually best splits the constituent objects of interest. This is under the assumption that the constituent objects have a noticeable edge in between them. Formally, we define a cut $\mathbf{c}$ to be a path connecting A^* and B^* on $\mathbf{I}$, with either a 4- or 8-pixel connectivity. We then define the cost of cut $\mathbf{c}$ between points A^* and B^* to be $E(\mathbf{c}) = \sum_{i=1}^{L} 1/e(\mathbf{I}(\mathbf{c}_i))$, where $\mathbf{c}_i$ represents the position of a pixel at location i on the cut, and L is the length of $\mathbf{c}$. Therefore, an optimal cut $\mathbf{c}^*$ minimizes cut cost $E(c)$, i.e.:

$$\mathbf{c}^* = \arg\min_{\mathbf{c}} E(\mathbf{c}) = \arg\min_{\mathbf{c}} \sum_{i=1}^{L} \frac{1}{e(\mathbf{I}(\mathbf{c}_i))}. \tag{3.4}$$

Interestingly, minimizing $E(\mathbf{c})$ is equivalent to finding the weighted shortest path between points A^* and B^* on $\mathbf{I}$. In our implementation, we apply the Dijkstra algorithm [26] to solve this shortest path problem.

Energy function (3.3) could also be written in different ways [7], as long as it captures the edge information from the original image. In our experiments, we only used gradient-based edge strength defined in (3.3). It is also obvious that when edge information is not adequate, the cut between points A^* and

B^* found by (3.4) will degenerate to the shortest Euclidean distance between them, which is the equivalent result to most existing methods.

3.5 Experimental Results

As mentioned, in our methodology, we first perform offline training for shape classification. The training and testing data sets consist of shapes extracted from images of the four application domains: oil said ore images, yeast cell images, blood cell images and curvalaria cell images. Then, we build our training set for each type of objects separately. Once trained, our method can then perform clump splitting online.

This section presents an evaluation of our method and compares its performance with three other clump splitting methods: (1) Kumar *et al.*'s rule-based splitting methods (RB) [48], (2) Farhan *et al.*'s improved clump splitting method (IM) [30], which is based on [48], and (3) the classical watershed-based method (WS) [13]. We choose to compare with these methods because RB is one of the most successful concavity based clump splitting methods that has been tested in various applications. IM is included due to its claim of being more accurate than RB. WS is used as the baseline method.

The implementations of IM [30] and the watershed method are based on the implementation from the author's website [30]. The implementation of the rule based method is based on the modification of IM. Finally, BN for bottleneck refers to our proposed bottleneck method.

3.5.1 Training and Testing for Shape Classification

To ensure robust clump splitting, we require a training set for each of the four applications. We randomly choose a training set that contains objects of different sizes and shapes. Specifically, we have 50, 30, 30 and 28 training shapes for each of the applications. Each training set has half positive and

half negative shapes (split/no-split cases). For testing, we have 649, 120, 257 and 50 testing objects for each of the applications.

It should be pointed out that, for each of the four types of images, we build a specific shape classifier based on shape features of solidity, convexity, eccentricity, area and variance on radius vectors. These features are used as the inputs to an SVM classifier. In our experiments, we used the libsvm package [17] for implementation.

We compare the accuracy from our shape classification to three other clump splitting methods in Table 3.1. Accuracy is defined as the total number of correctly labeled connected components as split/no-split cases over the total number of connected components in the testing data set. The details of evaluation metrics are described in Section 2.4.1 on page 29.

The results in Table 3.1 show that our shape classification method achieves a much better accuracy in all image sets. Especially for the segmentations of oil sand images, our method achieve much better accuracy due to very different shapes and sizes in oil sand objects compare to cell objects. We will also show in the next section that our method outperforms the competing methods in the splitting point detection step as well, which makes the overall performance even better in Table 3.2 and Table 3.3.

Table 3.1: Accuracy comparison between our shape classification method and three other competing methods in terms of identifying split/no-split cases.

Image set	**WS [13]**	**RB [48]**	**IM [30]**	**Our method**
Oil sands	64%	66%	68%	86%
Yeast cells	88%	81%	81%	90%
Blood cells	87%	88%	88%	90%
Curvalaria cells	72%	86%	88%	88%

3.5.2 Implementation of Clump Splitting

After shape classification, connected components which are determined to be clumps will go through the second and third steps of our method: splitting via bottleneck detection and cutting between the detected points. Each time when new objects are generated as the result of splitting, they will go through the shape classification step again until no more new clumps are found, as described in Figure 3.2. In this section, we will demonstrate some visual and quantitative results and compare our results with three competing methods.

3.5.2.1 Visual Results

Visual results are shown in Figure 3.5, where the first row shows six input clumps, the second to fourth rows show the splitting results from the three competing methods, and the fifth row shows the results from our method. We can see that our bottleneck-based method works for situations when points for splitting include non-concave points, or when concave points with very high concavity values are not the optimal candidate positions for splitting. It is also clear that IM (row 4) tends to over-split. This is because IM takes multiple points in one concavity region to avoid under-segmentation. In the case of watershed (WS, row 2), over-split occurs some times and under-split some other times. For cases when objects heavily overlap, watershed tends to under-split. Another significant difference between our method and the rest of the methods is shown in column (d), where while the other methods can only split clumps based on points on the contour of the clump, our method can successfully split connected components with other points inside the original clump, which is possible for heavily overlapped clumps.

Another group of visual results are shown in Figure 3.6 to demonstrate the effectiveness on multiple splitting cases only. We show the examples only from the applications of oil sand ore images and yeast images because the multi-

ple splitting cases are more complicated in these two applications, in which existing concavity based methods easily fail. Similarly, we can see that our bottleneck-based method works for situations when points for splitting include non-concave points, or when concave points with very high concavity values are not the optimal candidate positions for splitting. Our shape classification step helps in stopping the splitting procedure so that the algorithm does not over-split the clumps.

Figure 3.7 demonstrates the advantage of our method in connecting bottleneck positions. Row 1 shows four example input images, row 2 shows the cuts of these clumps with a straight line, and row 3 shows the cuts by our method which exploits image intensity information. Clearly, available edge information is helpful for accurate clump splitting, compared to connecting two points with the shortest Euclidean distance. Especially for column (b), in the third row, with edge based splitting, one newly split component has a more obvious bottleneck shape than the results from the other methods and leads to the next split successfully, while in the second row, a straight cut misleads the next split and results in a cut that prevents the next clump splitting from happening. For clumps in which edge information is missing between objects, our split algorithm then provides a straight cut between each pair of splitting points.

3.5.2.2 Quantitative Results

The overall performance of the clump splitting is evaluated quantitatively using two metrics: (1) the overall accuracy, as defined in Section 2.4.1 on page 29 ; (2) the probability of correct detection (PCD), which is defined as the percentage of correctly split clumps [8], i.e., the number of correctly split clumps divided by the total number of clumps that need to be split. Formally, let C stands for the total number of correctly split clumps and T stands for

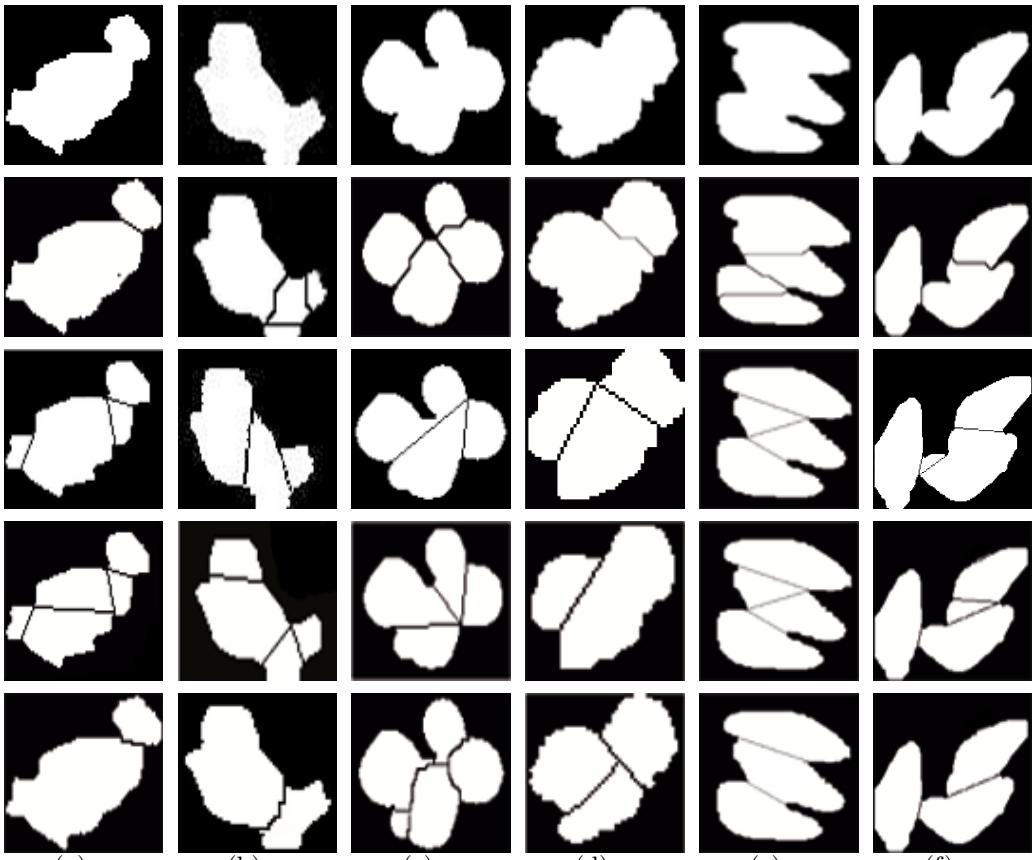

Figure 3.5: Visual results for clump splitting. The first row shows the original segmentation, the second row shows the splitting results from watershed algorithm (WS), the third row shows the splitting results from Kumar's concavity based method (RB) [48], the fourth row shows the results from the improved method (IM) [30] and the last row shows our results (BN). Column (a) and (b) are oil sands, column (c) is yeast cell, column (d) is blood cell, column (e) and (f) are curvalaria cells. We only show one example for yeast cell and blood cell because their shapes are very similar.

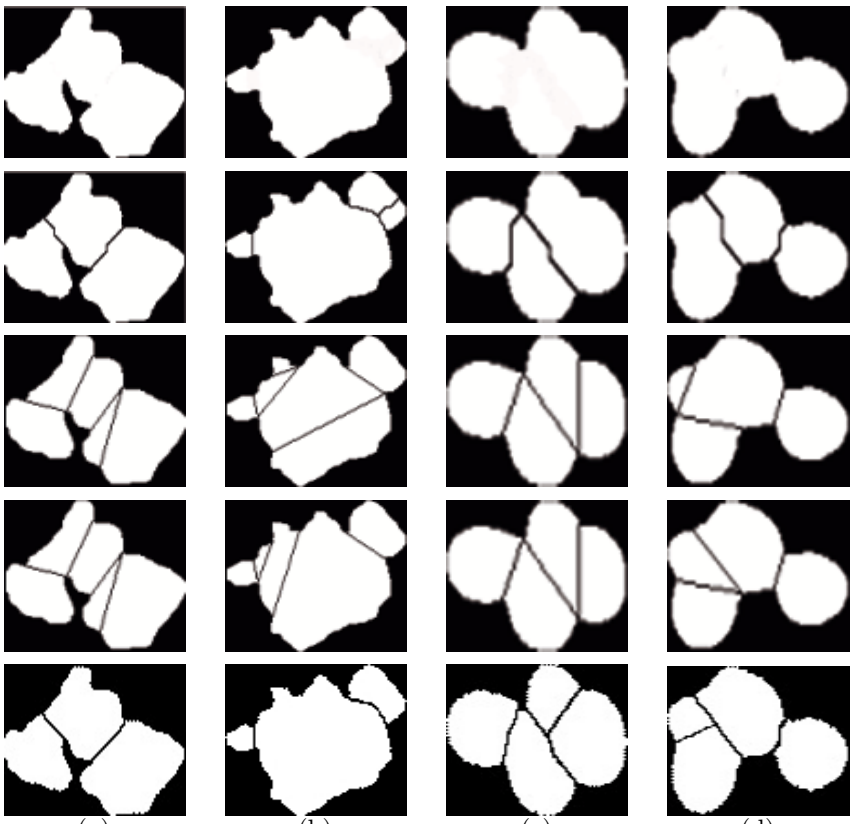

Figure 3.6: Visual results for multiple splitting cases. Row 2 through 5 show the original segmentation, the splitting results from watershed algorithm (WS), the splitting results from Kumar's concavity based method (RB) [48], the results from the improved method (IM) [30] and our results (BN), respectively. Column (a) and (b) are oil sands, and column (c) and (d) are yeast cells. WS and our BN work better than the competing RB and IM methods. In addition, WS could produce comparable results to ours only if the stopping criterion is carefully tuned, to avoid over or under-segmentation.

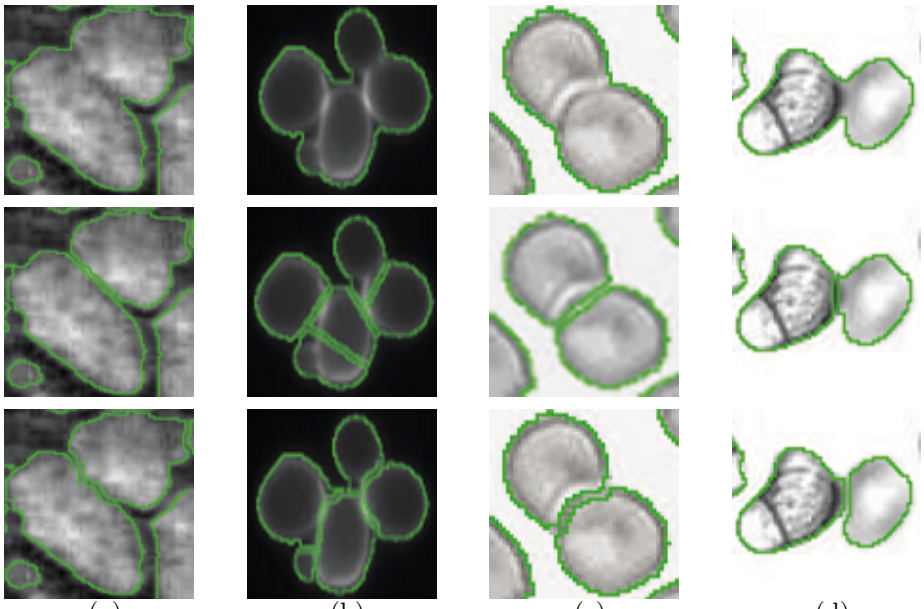

(a) (b) (c) (d)

Figure 3.7: Visual comparison between a straight cut and our weighted shortest path cut. The top, middle and bottom rows show the original images with the segmented boundary, the splitting results using bottleneck detection with straight cut, and the splitting results using our weighted shortest path cut. The segmented boundaries are shown in green. Column (a), (b), (c) and (d) are from oil sand images, yeast cell images, blood cell images and curvalaria cell images respectively.

the total number of clumps that need to be split, we have:

$$PCD = \frac{C}{T}. \tag{3.5}$$

Figure 3.8 clearly demonstrates how PCD is different from *accuracy*. In Figure 3.8, (a) shows the input to the splitting algorithm, while (b) shows the output. We have in total 15 connected components in (a), of which 5 are clumps. In (b), 1 out of the 5 clumps is correctly split, while 11 out of the 15 connected components are correctly handled. Therefore, we have $PCD = 1/5$, and $accuracy = 11/15$. This example shows how the two metrics measure performance in their own ways and why a high *accuracy* (11/15) does not guarantee a high PCD (1/5), especially in images where the majority connected components are not clumps. Intuitively, PCD helps to measure the

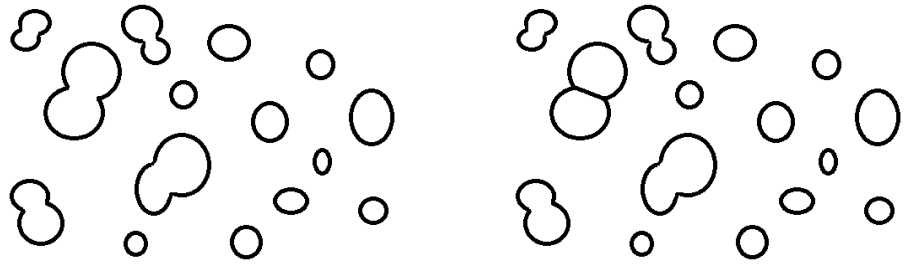

(a) (b)

Figure 3.8: An example on how PCD and accuracy are calculated. (a) shows the input to the splitting algorithm while (b) shows the output. There are in total 15 connected components in (a), in which 5 of them are clumps. In (b), 1 out of the 5 clumps is correctly split, while 11 out of the 15 connected components are correct. Therefore, we have $PCD = 1/5$, and $accuracy = 11/15$. This shows that a high *accuracy* (11/15) does not guarantee a high PCD (1/5), especially in images where the majority connected components are not clumps.

effectiveness of the splitting step only, while *accuracy* helps to measure the effectiveness of the whole algorithm including shape classification.

The results in terms of PCD and the overall accuracy are presented in Table 3.2 and Table 3.3, respectively. From both tables, we can see that in most application domains BN obtains significantly higher accuracies and PCDs than the competing methods. This is mostly because our method does not begin with locating concave points and then evaluating all of them in order to find the splitting points, but rather we find one pair of points that best represent the bottleneck positions of the component. Therefore, our method has a great advantage in splitting cases in which one or both of the points are not necessarily concave points, or are not concave points with the highest concavity value.

In addition, when comparing the results between Table 3.2 and Table 3.3, we can see that results of PCD reflect more on how accurately the clumps are split, which affects the overall performance of each method. When we compare Table 3.3 with Table 3.1, we can see that our method (BN) reaches a much

better performance when compared with the competing methods, especially in the oil sand, yeast cell and curvalaria cell data sets. In many cases, BN succeeds while the other methods generally fail when clumps with multiple objects heavily overlap. Compared with RB and IM, BN does not determine the number of splits by evaluating all pairs of split points and split lines, which are local measurements, but rather by considering the clump shape globally. Our shape classification method also has an advantage in terms of its flexibility to deal with various types of object classes expected in the clump splitting applications.

Table 3.2: Probability of correct detection (PCD) for four image sets. We compare our bottleneck detection method (BN) with watershed method (WS), Kumar's rule based method (RB) and Farhan's improved method (IM) in the table.

Image set	**WS [13]**	**RB [48]**	**IM [30]**	**BN**
Oil sands	22%	36%	39%	83%
Blood cells	70%	54%	56%	72%
Yeast cells	48%	61%	74%	83%
Curvularia cells	32%	58%	47%	60%

Table 3.3: Overall accuracy for four image sets. We compare our bottleneck detection method (BN) with watershed method (WS), Kumar's rule based method (RB) and Farhan's improved method (IM) in the table.

Image set	**WS [13]**	**RB [48]**	**IM [30]**	**BN**
Oil sands	60%	59%	62%	86%
Yeast cells	58%	56%	60%	80%
Blood cells	86%	86%	87%	87%
Curvalaria cells	47%	62%	66%	70%

3.6 Summary

In this chapter we have proposed a novel framework to perform clump splitting. The proposed method consists of three steps: (1) decide whether to split a candidate connected component by shape classification; (2) find a pair of points for clump splitting and (3) join the pair of selected points. In the first step, an application-specific shape classifier is applied to determine whether a connected component should be split. In the second step, a pair of points for splitting is detected using an application-independent bottleneck rule, under the assumption that the desired objects have roughly a convex shape. We acknowledge that clump splitting in general is a research topic of broad interest in image processing where this assumption may not hold, and that our proposed algorithm should not be considered as general for splitting objects of arbitrary shape. In the third step, the selected splitting points for step two are joined by finding the optimal splitting line between them, based on minimizing an image energy, again in an application-independent manner. The shape classifier is built offline via various shape features extracted from training shapes in each application and a support vector machine.

The proposed method has several advantages over existing methods. First, our method is not parameter-dependent on finding candidate points for splitting, unlike most existing methods, especially concavity based methods, which are highly parameter-dependent. Our method is global and always finds the bottleneck of a clump, which gives the best positions for splitting a convex-shaped clump. Second, our method avoids dealing with special situations in which splitting points are not concave. In these cases, almost all existing methods need to add extra points according to the heuristic rules and constraints. Our method, on the other hand, avoids this issue by finding the optimal pair of points, instead of one point at a time. Furthermore, our method takes in-

tensity information into account in localizing the cut between splitting points and finds a more accurate cut than the straight-line cut that directly joins the splitting points. Finally, the proposed method makes use of shape classification to determine which connected components are clumps and the number of splits for each clump, and it is therefore more flexible than model based methods. We have validated our method in four different application domains and have shown its better robustness and accuracy in clump splitting than the state-of-the-art algorithms for this important problem in image segmentation.

The proposed clump splitting method can be easily incorporated in an interactive segmentation framework. Admittedly in an interactive segmentation framework, the decision of whether to split a connected component can be made by the user interactively, our proposed shape classification method can also help in automated segmentation applications. In Chapter 5 we will describe how to integrate this clump splitting method into an interactive segmentation framework.

Chapter 4

Boundary Refinement via Shape PCA Method

This chapter presents the third contribution of this dissertation, namely the shape PCA method. In order to refine the boundary of the incorrectly segmented objects at the final stage of an image segmentation task, the shape PCA method takes advantage of statistical shape information and refines the shape of an incorrectly segmented object with the first few principal components, which presumably represent the true shape of the object. This chapter will first review some background on statistical shape analysis, focusing on two dimensional shape representation, shape alignment and some existing statistical shape models. Then, principal component analysis (PCA) and our proposed shape PCA method will be described followed by experimental results validating its effectiveness.

4.1 Introduction

Shapes are one of the basic and important visual features used to describe image content. The shape of an object is a geometrical description of such an object in a certain dimensional space, as determined by the object's external boundary. Mathematicians define shape as "all the geometrical information that remains when location, scale and rotational effects are filtered out from an object" [27]. In other words, a shape is not dependent on geometrical transformations such as translation, scaling and rotation. Shapes can often be described by basic geometry primitives such as points, lines, curves, etc.

Shape analysis is a difficult task in computer vision. When a three dimensional object in the real world is projected onto a two dimensional plane, one dimension of the shape information is lost. A shape extracted from digital images is generally the projected 3-D object on a 2-D plane. What is worse, the shapes we obtained from an digital image are often corrupted with noise, occlusion, distortion, etc.

Statistical shape analysis is a geometrical analysis from a set of shapes

via statistical measures, to describe the geometrical properties among similar shapes. Statistical shape analysis is now widely used to represent and analyze various shapes. Before describing our proposed shape PCA method in Section 4.3, we will first present some preliminaries and existing methods in statistical shape analysis.

4.2 Statistical Shape Analysis

4.2.1 Shape Representation

One of the first steps after collecting a set of shapes is to apply a proper shape representation scheme for further statistical analysis. Shapes are generally represented by effective and important shape features based on the boundary of the shape, or both shape boundary and interior content of the shape. In this dissertation, only two dimensional objects are considered. It is generally assumed that the 2D information is sufficient for a reasonable characterization of shapes [43].

There are different description techniques for categorizing shapes. Some categorize them into contour-based and region-based methods [99]. This categorization is based on whether the shape features are extracted from the contour of the shape only, or from the whole shape region. Under each class, different methods can be categorized further into structural approaches or global approaches. This sub-class is based on whether the shape is represented as a whole or represented by sub segments/sections of the shape. These approaches can be even further distinguished into space domain or transform domain.

Another way of categorizing shape representation techniques is to divide them into functional approaches, set theory approaches, and point/landmark approaches, each of which is based on how shapes are described mathematically [43]. The functional methods describe shapes in terms of contour func-

tion, radius vector function, support function, width function, tangent-angle function, etc. The set theory approaches, on the other hand, represent shapes in terms of simple geometrical parameters such as area, perimeter, convex hull, area-perimeter ratio, different roundness ratios, convexity ratio, etc. The third types of techniques, which are one of the most commonly used techniques in shape representation, describe shapes by a set of points which usually lie on the contour of the shapes and are defined by some geometrical properties or have a certain physical meaning. Such methods are also called landmark based techniques.

In statistical shape analysis, one of the most popular shape representation methods is to locate a finite number of coordinate points which are called landmarks on the contour of a shape. A landmark is defined as a point of correspondence on each object that matches between and within a group of similar objects [27]. Landmarks are sometimes also called vertices, control points, dominant points, nodes, markers, etc. Given a set of similar shapes in a computer vision task, for each shape, a set of landmark points are extracted using one or a combination of shape representation techniques. The extracted landmark points must be consistent from one shape to another.

There are generally three types of landmarks: anatomical landmarks, mathematical landmarks and pseudo landmarks. An anatomical landmark is a point assigned by an expert that corresponds between organisms in some biologically meaningful way [27]. For example, the corners on the contour of an eye or the joint point between two lungs are anatomical landmarks. Mathematical landmarks are points located on an object which corresponds to some mathematical or geometrical property of the shape. For example, dominant points which are found on the high curvature positions on a contour of a shape are mathematical landmarks. Pseudo landmarks are constructed points located between anatomical or mathematical landmarks. Figure 4.1 shows an exam-

ple of landmarks located on the contour of an airway on an airway image. On the airway, the white diamonds around crosses are mathematical landmarks, and the red crosses only are pseudo landmarks.

Figure 4.1: Example of landmarks on the contour of an airway on an airway image. On the airway, the white diamonds around crosses are mathematical landmarks, and the red crosses only are pseudo landmarks.

4.2.2 Shape Alignment

Finding a meaningful correspondence between two or more than two shapes is a fundamental step before shape analysis can be properly performed. In such a task, the goal is to find an explicit relationship between a group of similar shapes. Finding such a matching involves searching through all possible shape alignments [12]. Shape alignment is one of the solutions for shape matching by performing transformation search. In statistical shape analysis, finding alignment between shapes is formulated as an optimization problem over matched landmarks. In this section, we will introduce two basic and popular shape alignment techniques: Procrustes analysis [27] and congealing [49].

4.2.2.1 Procrustes Analysis

The most popular method to align shapes in statistical shape analysis is the generalized Procrustes alignment (GPA) [27]. The standard Procrustes match minimizes the mean squared distance between two shapes. To align a group of shapes to their mean shape, this procedure runs iteratively, resulting in the generalized Procrustes alignment (GPA) [37, 81]. In the following sections we will describe Procrustes distance and GPA.

Procrustes Distance

The Procrustes distance [27, 28, 15, 21] is a type of shape metric that requires two aligned shapes to have one-to-one point correspondence. The alignment process involves four steps as follows.

1. Compute the centroid of each of the shapes.
2. Normalize the two shapes to have the same size.
3. Align the two shapes at the centroids with regard to their positions.
4. Align the shapes with regard to their orientations.

After performing the four steps above, the squared Procrustes distance between two shapes A and B is simply the sum of the squared point distances. Let the landmark coordinates for shape A and B be $A = (x_{Ai}, y_{Ai})$, and $B = (x_{Bi}, y_{Bi})$, $i = 1...n$, where n represents the total number of landmarks on the border of each shape. The squared Procrustes distance between shape A and B is therefore:

$$P_d^2 = \sum_{i=1}^{n} [(x_{Ai} - x_{Bi})^2 + (y_{Ai} - y_{Bi})^2]. \tag{4.1}$$

Generalized Procrustes Alignment

To align a group of shapes to their mean shape, the standard Procrustes match procedure run iteratively, resulting in the generalized Procrustes alignment.

The following iterative approach describes the generalized Procrustes analysis procedure [81].

1. Choose an initial estimate of the mean shape (e.g. the first shape in the set).

2. Align all the remaining shapes to the mean shape.

3. Re-estimate of the mean from the aligned shapes.

4. If the estimated mean has changed return to step 2.

When the mean shape does not change significantly within an iteration, the above procedure converges.

4.2.2.2 Congealing

Among existing shape alignment methods, congealing is a flexible nonparametric data-driven framework for the joint alignment of a set of shapes. Congealing has been successfully applied to the joint alignment of binary, gray scale and color images [49].

Congealing is defined with respect to a set of transformations. For the purpose of shape alignment, congealing is applied by taking a set of images and transforming them according to a continuous set of allowable transformations to make them more similar, according to the measure of similarity. It works by parameterizing the set of transformations composing of x-translation, y-translation, rotation, x-scale, y-scale, x-shear and y-shear. Thus, given a parameter vector $v = (t_x, t_y, \theta, s_x, s_y, h_x, h_y)$, a transformation matrix U is formed by:

$$
\begin{aligned}
U &= F(t_x, t_y, \theta, s_x, s_y, h_x, h_y) \\
&= \begin{bmatrix} 1 & 0 & t_x \\ 0 & 1 & t_y \\ 0 & 0 & 1 \end{bmatrix} \begin{bmatrix} \cos\theta & -\sin\theta & 0 \\ \sin\theta & \cos\theta & 0 \\ 0 & 0 & 1 \end{bmatrix} \\
&\quad \begin{bmatrix} e^{s_x} & 0 & 0 \\ 0 & e^{s_y} & 0 \\ 0 & 0 & 1 \end{bmatrix} \begin{bmatrix} 1 & h_x & 0 \\ 0 & 1 & 0 \\ 0 & 0 & 1 \end{bmatrix} \begin{bmatrix} 1 & 0 & 0 \\ h_y & 1 & 0 \\ 0 & 0 & 1 \end{bmatrix}
\end{aligned}
$$

Note that this is an over-complete parameterization in order to allow the congealing algorithm to move easily toward an optimum because the implementation of coordinate descent algorithm [49].

For the similarity objective function, congealing works by optimizing the objective function which is defined as

$$E = \sum_{i=1}^{P} \hat{H}(x_i') + \sum_{j=1}^{N} |v^j|^2 \tag{4.2}$$

where $\hat{H}(x_i')$ is an entropy estimation term for measuring the similarities between images (in our case shapes) and v^j is a transform parameter vector which penalizes large transformations away from the initial position. $\hat{H}(x_i')$ is defined as empirical entropy of the set of values in the pixel stack

$$\hat{H}(x_i') = -(\frac{N_0}{N}\log_2\frac{N_0}{N} + \frac{N_1}{N}\log_2\frac{N_1}{N}) \tag{4.3}$$

where N_0 and N_1 are the number of occurrences of 0 (black) and 1 (white) in the binary-valued pixel stack [49].

By optimizing the objective function E described in Equation (4.2), congealing make a set of shapes more similar to each other by independently transforming each one of them in an affine manner. Therefore, a group of shapes are properly aligned after congealing converges.

4.2.3 Statistical Shape Models

For model-based segmentation approaches, creating a proper shape model is one of the last but important steps after the steps of collecting a set of shapes, using a proper shape descriptor to represent each of the shapes, and aligning them with an alignment technique. In the last two decades, model-based segmentation approaches have been established as one of the most successful methods in image analysis. By matching a statistical model which contains shape information about the expected shape in the new images, image segmentation algorithm is performed. These shape based algorithms are more robust

compare to algorithms which only segment an image based on image intensity information. Considering the variability of the objects of similar shapes, information about shape variations can be included in a shape model. Statistical shape model is such an approach to collect statistical shape information including shape variations via a number of sample shapes.

Constructing a statistical shape model basically consists of extracting the mean shape and a number of modes of variation from a collection of samples. Due to the dominant role and simplicity in landmark-based representation, we concentrate on landmark-based models in this section. Given a set of such examples, we first align them into a common Euclidean coordinate system using shape alignment techniques such as GPA or congealing. Once aligned, different statistical shape models can be applied. In the following section, some background on principal component analysis (PCA) will be presented, followed by the description of Active Shape Model.

4.2.3.1 PCA and Related Work

Principal Component Analysis (PCA) [44] is a standard method in a variety of applications to find out inherent data structure. It refers to a mathematical procedure that applies orthogonal transformation to convert a set of originally possibly correlated variables to a set linearly uncorrelated variables. The linearly uncorrelated variables are defined as principal components. The principal components represent the major directions of variability in the dataset and are described by the eigenvectors. The orthogonal transformation generates principal components in such a way that the first principal component has the highest variance.

Principal Component Analysis (PCA) has been used widely in the literature for modeling shape variations for traditional statistical shape analysis. Cootes *et al.* [23] introduced the Active Shape Model (ASM). On the other

hand, Active Appearance Model (AAM) is introduced as a generative model that can synthesize images similar to those in the training set [20]. Typically, AAM is used for image interpretation and syndissertation applications. Using a set of training images, both shape and texture of the object of interest are modeled. Therefore, image interpretation tasks can easily fit a new unseen image into the model.

Moreover, Cootes *et al.* [22] developed PCA in the tangent space for statistical shape analysis. They [23, 22, 19] applied PCA and built a point distribution model (PDM) to describe the variability in shape, which is a model for shape and uses Procrustes residuals. Based on this two-dimensional formulation of shape PCA, Wang *et al.* [93] proposed an approach for boundary detection where shape priors and edge information of the input image are incorporated. However, these methods encounter difficulties for cases when edge information is weak, or when objects have occlusions. To deal with these situations when edge information is very weak or totally missing, we propose the shape PCA method in Section 4.3. Before getting into the details of our shape PCA method, we will give some related background on a specific statistical shape model: active shape model.

4.2.3.2 Active Shape Model

Cootes *et al.* introduced the Active Shape Model (ASM), which is a deformable model that globally constrains the deformation of a shape to valid instances of the object of interest [23]. The shape constraint normally improves the model and provides better segmentation. The ASM algorithm consists of three major steps: (i) generating Point Distribution Model (PDM), (ii) generating Local Appearance Model (LAM), and (iii) model search procedure. We will describe each of the major steps briefly in this section.

Point Distribution Model

The point distribution model (PDM) is a model for representing the mean geometry of the shape and some statistical modes of geometric variation inferred from a set of training shapes. It is the first and most crucial step for the ASM algorithm.

Let the contour of an object be represented by a fixed number of labeled landmarks $p_i = (x_i, y_i), i = 1...n$. Prior to modeling the shape variations in the training set, we assume that they are already aligned with respect to translation, rotation and scaling via a shape alignment method. Non-rigid variations are then modeled by using the PDM. PDM uses principal component analysis (PCA) to capture the second-order statistics in the training set. The PDM represents a shape as a mean shape plus a weighted sum of basic functions defined as the eigenvectors of the covariance matrix. Formally, the mean shape is defined as:

$$\bar{\mathbf{x}} = \frac{1}{N}\sum_{i=1}^{N}\mathbf{x}_i. \tag{4.4}$$

where N stands for the number of shapes and $\mathbf{x}_i$ denotes the ith shape. The covariance matrix is

$$S = \frac{1}{N-1}\sum_{i=1}^{N}(\mathbf{x}_i - \bar{\mathbf{x}})(\mathbf{x}_i - \bar{\mathbf{x}})^T. \tag{4.5}$$

The eigenvector φ_k and eigenvalues λ_k of S are therefore computed as:

$$S\varphi_k = \lambda_k\varphi_k. \tag{4.6}$$

Since the matrix of the eigenvectors $\phi = [\varphi_1\varphi_2...\varphi_N]$ represents the modes of variations of the shapes, normally the variations in the training set can be described by a small number of modes. Therefore, a good estimation of the shape can be obtained by retaining the eigenvectors φ_i that correspond to the t largest eigenvalues:

$$\mathbf{x} = \bar{\mathbf{x}} + \phi\mathbf{b} \tag{4.7}$$

where $\phi = [\varphi_1 \varphi_2 ... \varphi_N]$ and $\mathbf{b}$ is a t dimensional vector given by

$$\mathbf{b} = \phi^T(\mathbf{x} - \bar{\mathbf{x}}). \tag{4.8}$$

The vector $\mathbf{b}$ defines a set of parameters of a deformable model [18].

PDM can be extended to any arbitrary number of dimensions, but is typically used in two dimensional image and three dimensional volume applications.

Local Appearance Model

During the training phase of constructing ASM, a local appearance profile is constructed for every landmark point on the contour. The main idea is to examine the image level information in a region on the original image around each landmark throughout the training set. Given a training set of N_p images, the local appearance profile is constructed as follows. Assuming we are dealing with gray scale images, for every landmark point j in the image i of the training set, a gray level profile $\mathbf{g}_{ij}$ is extracted, of length n_p pixels, centered around the landmark point. Here the actual gray level profile from the image is not used, but its normalized derivative. This gives invariance to the offsets and uniform scaling of the gray levels.

Therefore, the gray level profile of the landmark j in the image i is a vector of n_p intensity values:

$$\mathbf{g}_{ij} = [g_{ij0} g_{ij1} \dots g_{ijn_p-1}]^T \tag{4.9}$$

and the normalized derivative of the gray level profile is

$$\mathbf{y}_{ij} = \frac{d\mathbf{g}_{ij}}{\sum_{k=0}^{n_p-2} |d\mathbf{g}_{ijk}|} \tag{4.10}$$

where $\mathbf{dg}_{ij} = [g_{ij1} - g_{ij0}, g_{ij2} - g_{ij1}, \dots, g_{ijN_p-1} - g_{ijN_p-2}]^T$.

Now the mean of the normalized derivative profiles of each landmark throughout the training set can be calculated. For each landmark j, the mean profile

$\bar{\mathbf{y}}$ and the covariance matrix $\mathbf{C}_j$ are:

$$\bar{\mathbf{y}}_j = \frac{1}{N}\sum_{i=1}^{N} d\mathbf{g}_{ij}, \tag{4.11}$$

$$\mathbf{C}_j = \frac{1}{N}\sum_{i=1}^{N}(\mathbf{y}_{ij} - \bar{\mathbf{y}}_j)(\mathbf{y}_{ij} - \bar{\mathbf{y}}_j)^T. \tag{4.12}$$

Model Search Procedure

After generating the PDM and LAM, the segmentation of the active shape model is finally achieved by fitting the learned model to a new image by estimating the model parameters $\mathbf{b}$ and the pose parameters (t_x, t_y, s, θ) that best fit the image:

$$\mathbf{x} = T_{t_x,t_y,s,\theta}(\bar{\mathbf{x}} + \phi\mathbf{b}). \tag{4.13}$$

$T_{t_x,t_y,s,\theta}$ is a function that translates the shape by (t_x, t_y), scales it by s and rotates it by θ. The initialized pose estimates are $(t_{x_0}, t_{y_0}, s_0, \theta_0)$. $\bar{\mathbf{x}}$ represents the mean shape. The model search iterates therefore as follows:

(i) For each landmark, examine a search profile along a line perpendicular to the contour and passing by the landmark. Find the location that best fits the learned local appearance profile of this landmark, i.e., the location that minimizes the Mahalanobis distance $h(\mathbf{y_s})$:

$$h(\mathbf{y_s}) = (\mathbf{y_s} - \bar{\mathbf{y}}_\mathbf{k})^T {\mathbf{S}_{\mathbf{y_k}}}^{-1}(\mathbf{y_s} - \bar{\mathbf{y}}_\mathbf{k}) \tag{4.14}$$

where $\mathbf{y_s}$ is the local appearance profile for the current position in the search, $\bar{\mathbf{y}}_\mathbf{k}$ and $\mathbf{S}_{\mathbf{y_k}}$ represent the local appearance model for the kth landmark, ${\mathbf{S}_{\mathbf{y_k}}}^{-1}$ denotes the inverse of the covariance matrix of $\mathbf{y}_i$.

(ii) Update the parameters $(t_x, t_y, s, \theta, \mathbf{b})$ to best match the new shape estimated from (i):

$$\mathbf{b} = \phi^T(\mathbf{x}_s - \bar{\mathbf{x}}), \tag{4.15}$$

$$\tilde{\mathbf{x}} = T_{t_x,t_y,s,\theta}(\bar{\mathbf{x}} + \phi\mathbf{b}). \tag{4.16}$$

4.3 Boundary Refinement via Shape PCA

One problem with current statistical models is that when image level information is inadequate or missing, the statistical models have difficulties converging to the correct segmentation. On the other hand, in an interactive segmentation scenario, when the user can tell that the image level information is inadequate or missing, so that existing statistical shape model based methods will have difficulties, a different method based only on statistical shape information should be applied to avoid such difficulties. Our proposed shape PCA method is developed with such motivation. Our shape PCA method is capable of not only refining the boundary of the desired object, but also improving the efficiency of the segmentation procedure by avoiding the model search procedure.

4.3.1 Shape PCA Projection

As mentioned, previous shape PCA methods in image segmentation incorporate statistical shape information as a prior term in the deformable shape model and iteratively achieve convergence in a segmentation process. Our method, on the other hand, exploits the assumption that the major principal components (PCs) represent the true shape and the residual error from shape PCA represents segmentation errors and thus should be removed in order to obtain satisfying segmentation results. The geometric shape information is represented using landmarks on the contour of the shape, based on two dimensional formulation. Shape PCA is subsequently applied to extract relevant information, under the assumption that a correctly segmented shape should be similar to those previously seen in the training set.

To be more detailed, the shape PCA method consists of a training phase and a testing phase. For both the training and the testing phase, we first convert the geometric shapes into a numerical representation. Since we choose

landmark based representation in our experiments, this procedure is typically done by identifying or placing landmarks along the shape boundary. To illustrate it in a simple way, in our experiments, we evenly place a fixed number of landmarks along the boundary of the aligned shape, which is done in a similar way in existing work such as [23]. Here we assume that all the shapes are aligned already, by either procrustes analysis or congealing.

In the training phase, given m aligned shapes, each of which with a set of n landmarks, we can calculate the mean shape and the covariance matrix. Each of the aligned shapes can be represented as:

$$L_i = [x_i(1), x_i(2), \ldots, x_i(n), y_i(1), y_i(2), \ldots, y_i(n)]^T \tag{4.17}$$

where $i = 1, ..., m$, $x_i(k)$ and $y_i(k)$ denote the x and y coordinates of the kth landmark position in the two dimensional Euclidean space. After performing PCA on the aligned shapes in the training set, we let PC_j represent the jth principal component.

In the testing phase, when a new testing shape comes which needs boundary refinement, in order to reconstruct a new shape, we can perform PCA projection by using only a selected number of the principal components. Theoretically, the first few largest eigenvectors usually describe the most significant modes of variations of the shapes which belong to the same category. We can therefore reconstruct a new shape in the reprojection process by not using the rest of the PCs which presumably mostly represent unwanted parts of the shapes. Following this assumption, we have

$$L_i^g = \sum_{j \in S_{PCA}} (PC_j \cdot w_j) \tag{4.18}$$

where $L_i^g = [x_i'(1), x_i'(2), \ldots, x_i'(n), y_i'(1), y_i'(2), \ldots, y_i'(n)]^T$ represents the reconstructed shape, S_{PCA} is a subset of $\{1, \ldots, m\}$, which represents the indices of selected principal components, and $w_j = PC_j^T L_i$.

4.3.2 Algorithm for Shape PCA

As mentioned, the proposed shape PCA algorithm consists of two parts, training (left column of Figure 4.2) and testing (right column of Figure 4.2). The training part where PCA is performed to learn object shapes consists of the following steps:

1. **Obtain training shapes.** This can be done from a collection of ground truth images which are manually labeled by experts.

2. **Align all the extracted shapes.** Before shape alignment, the same number of landmarks are placed evenly on the perimeter of each of the aligned training shapes. Then the alignment can be done by different shape alignment methods. In our experiments we choose congealing (see Section 4.2.2.2) because it is efficient and optimal, although similar results could be obtained by Generalized Procrustes Alignment.

3. **Perform principal component analysis on the training shapes.**

To apply the extracted shape information from the training phase online, improvement for a given incorrectly segmented object consists of the following steps (we call them testing steps):

1. **Shape alignment.** This step performs similar landmark interpolation and shape alignment procedures as in the training phase.

2. **Shape PCA projection.** In this step, we choose a fixed number of principal components and perform PCA projection on the testing shape, which is the incorrectly segmented object.

3. **Obtain the segmentation results.** In order to obtain the final image segmentation result, the inverse procedure for the aligned shape should be performed, such as scaling, rotation, etc.

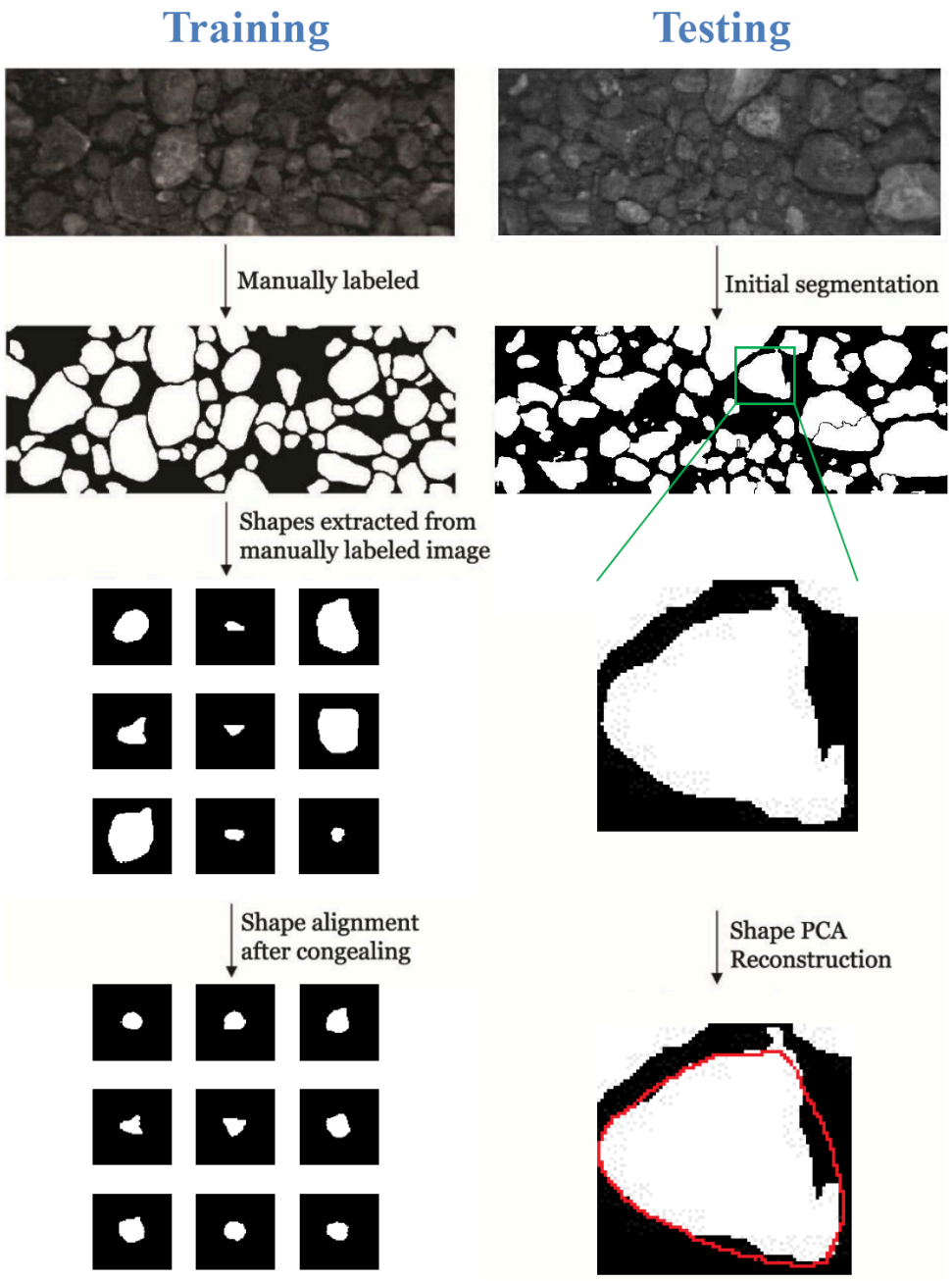

Figure 4.2: Flowchart of the proposed shape PCA algorithm, with examples on oil sand image segmentations. The left column in the figure shows the training steps, with training shapes extracted from manually labeled segmentation. The right column shows the testing steps with incorrectly segmented objects in the initial segmentation. The red boundary on the last image on the right column represents the improved segmentation after our proposed shape PCA method.

The general flowchart of the proposed algorithm is summarized in Figure 4.2 on page 76, with examples on oil sand image segmentations. The left column in the figure shows the training steps, with training shapes extracted from manually labeled segmentation. The right column shows the testing steps with incorrectly segmented objects in the initial segmentation. The red boundary on the last image on the right column represents the improved segmentation after shape PCA method.

4.3.3 Local Shape PCA

Refining the entire boundary of an object by shape PCA might modify some portions of already correctly delineated boundary of the object. Motivated by the observations that usually only parts of the object boundary are incorrect and the rest is correct, in this section, we further extend the shape PCA method to a *local* shape PCA method, in contrast to the *global* shape PCA method described in the previous section.

The difference between global shape PCA and local shape PCA is that, for global shape PCA, all landmarks on the shape boundary are refined by shape PCA, while for local shape PCA, only selected parts of the landmarks on the shape boundary are refined and the rest of the boundary remains the same. Note that for local shape PCA, we still calculate PCA projection on the whole boundary, but only the changes to the selected parts of the boundary are made. With the localizing method to be elaborated later in this section, after localizing the local incorrect boundary on the shape, the local shape PCA method can be performed as follows:

$$L_i^l(k) = \begin{cases} L_i^g(k), & \text{if } k \in S_{Local} \\ L_i(k), & \text{if } k \notin S_{Local} \end{cases} \tag{4.19}$$

where $L_i^g(k)$ represents the projected shape via shape PCA at the kth landmark position $(x_i(k), y_i(k))$ from Equation (4.18), $L_i(k)$ represents the original shape

at landmark position k, S_{Local} is the selected local sections of the boundary that need to be fixed, expressed as a subset of $\{1, \ldots n\}$.

To identify sections of the object boundary that should be improved or refined via shape PCA, we observe that in applications such as oil sand images and cell images, empirically there is a strong correlation between incorrect boundary delineation and frequent change in the polarity of the curvature. This change can be captured with the help of the radius-vector function [82] associated with the object boundary. Therefore, in order to localize inaccurate boundary, we focus on detecting local boundary with high variances of radius-vector function and select them as S_{Local} to perform local shape PCA.

To be more specific, after landmarks are placed evenly on the perimeter of the shape, we pick an arbitrary point O that is interior to the shape, and calculate the distances or radii from O to the landmarks. For a section of the boundary to be considered inaccurate or incorrect, the variance of the radii within that section must exceed a certain threshold, which is application-dependent. This calculation is then performed to all landmarks, and the sections which need to be corrected can then be identified and assigned to S_{Local} in Equation (4.19).

4.4 Experimental results

The shape PCA method has been implemented and tested on oil sand images [88]. Our experiment uses a set of nine oil sand images to validate the proposed approach for boundary refinment. The nine images are first segmented by human experts to establish ground truth. They are then sent to a watershed-based segmentation algorithm [53] to generate machine-segmented images, to be corrected by our shape PCA algorithm. The first ground truth image is used for training to obtain the PCs of expected shapes, and the remaining eight are used for testing.

When shape PCA is performed on the eight testing images, the number of principal components varies from one to the maximum number of principal components (74 in our experiments). We perform shape PCA for both global and local shape PCA and compare the statistical and visual results.

Figure 4.3 shows an example of visual results of how segmentations have been improved after performing shape PCA method on oil sand images. In Figure 4.3, (a), (b) and (c) are global shape PCA results with the selections of 3, 5 and 10 PCs while (d), (e) and (f) are local shape PCA results with the selections of 3, 5 and 10 PCs. The location within the green dashed box shows an example where local and global shape PCA perform differently. Figure 4.4 and Figure 4.5 show the statistical results of accuracy and score from both global and local shape PCA methods on oil sand images. The details of evaluation metrics are described in Section 2.4.1 on page 29

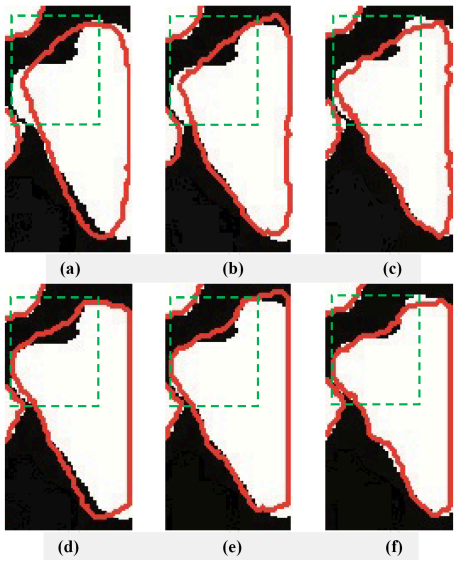

Figure 4.3: An example of visual results of how segmentations have been improved after performing global and local shape PCA methods on oil sand images. (a), (b) and (c) are global shape PCA results with the selections of 3, 5 and 10 PCs while (d), (e) and (f) are local shape PCA results with the selections of 3, 5 and 10 PCs. The location within the green dashed box shows an example where local and global shape PCA perform differently.

From both statistical and visual results, we can see that performing shape

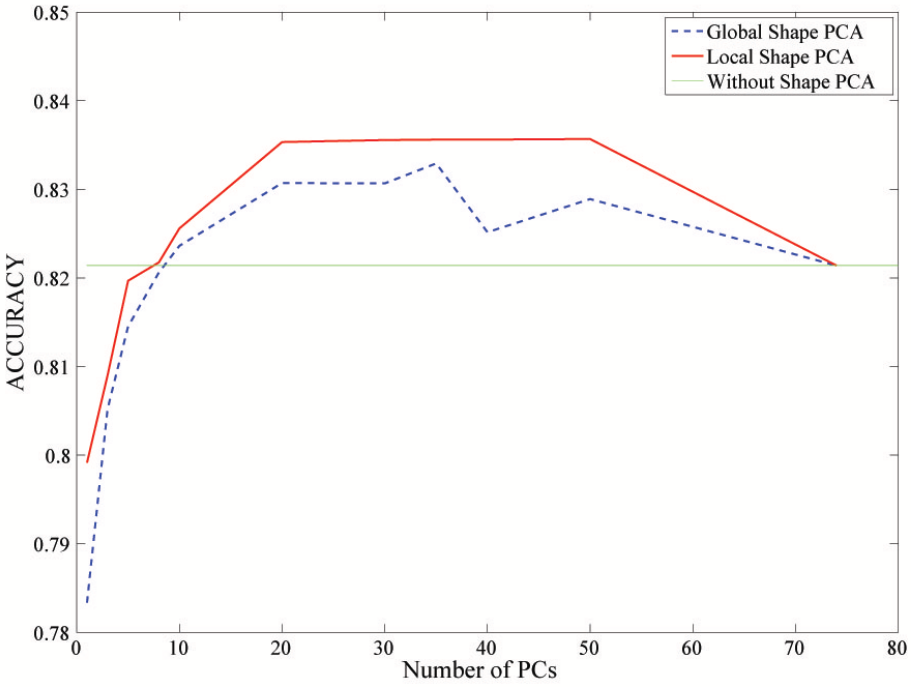

Figure 4.4: Statistical results of accuracy with both global and local shape PCA methods on oil sand images.

PCA as a boundary refinement step improves the final segmentation results, at both the pixel level and object level, when the number of principal components is properly chosen. In particular, local shape PCA produces a better and more stable performance than global shape PCA in general, as long as the incorrectly segmented sections of the object boundary can be correctly identified.

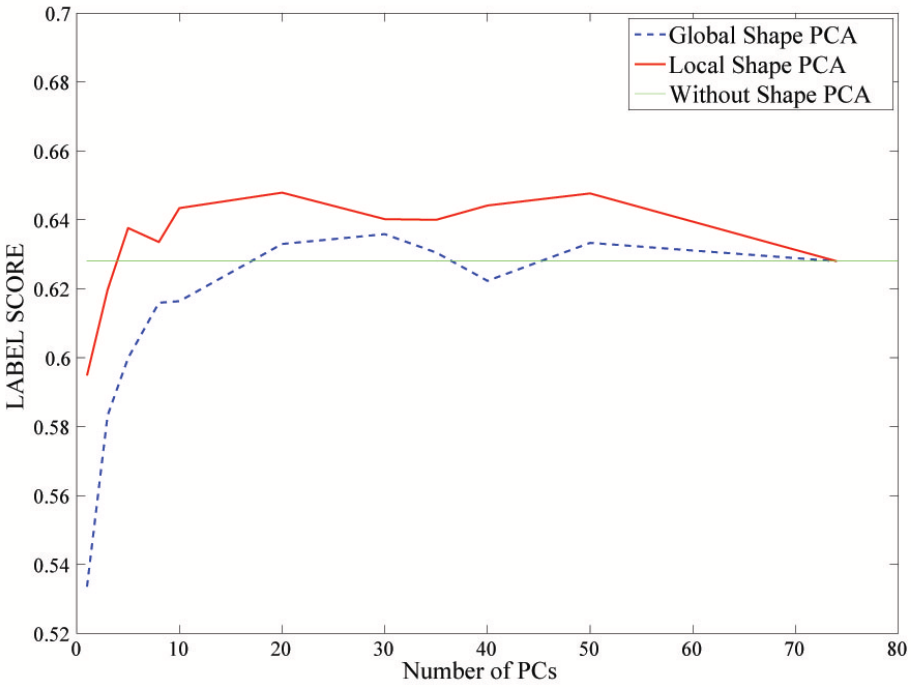

Figure 4.5: Statistical results of score with both global and local shape PCA methods on oil sand images.

Our experimental results are based on the application of oil sand image segmentations. However, because we make few assumptions, except that ground truth images are available and objects of interest share common shape characteristics, the proposed algorithm is not limited to this application. It could be easily applied to applications such as blood cell image segmentations, etc. As long as the incorrectly segmented sections of the boundary can be localized correctly, either automatically or manually, our shape PCA method can be utilized into the boundary refinement procedure in an segmentation task.

4.5 Summary

This chapter focuses on the last step of an image segmentation task: boundary refinement. We start approaching boundary refinement by statistical shape analysis. After reviewing some preliminaries and background on statistical shape analysis, the shape PCA method is proposed in this chapter. The shape PCA method takes advantage of shape information which is not directly available from image level. In the boundary refinement process, the shape PCA method refines the 0boundary of an object by using the first few principal components which presumably represent the true shape of the object. The local shape PCA method is also proposed to be compared with the global shape PCA method. As long as the incorrectly segmented portions of the object boundary can be localized correctly, either automatically or manually, local shape PCA can be easily applied to perform boundary refinement for incorrectly segmented objects. In Chapter 5 we will describe how to integrate the shape PCA method to an interactive segmentation system.

Chapter 5

An Interactive Image Segmentation System

This chapter introduces a comprehensive framework for interactive image segmentation, as an example to integrate the shape-guided segmentation algorithms developed in this dissertation. This interactive segmentation framework is composed of five tools, which are developed based on common cases of incorrect segmentations from any segmentation algorithms. From observation, most image segmentation tasks can be handled by a combination of these five actions. When combining all the shape-guided segmentation algorithms we proposed in the previous chapters, adaptive shape prior (ASP) method, clump splitting method via bottleneck detection, and shape PCA method, this interactive segmentation framework can be constructed into a highly effective and efficient interactive object segmentation system with minimal user input.

5.1 Purpose of User Interaction

As mentioned, user interaction is very crucial for obtaining desired segmentation results. As a general rule from the existing research, the purpose of interaction is to combine the expertise of a human operator and the power of a segmentation algorithm to obtain the desired delineation of the object in the image in an efficient manner [66]. Figure 1.2 has already demonstrated the general process of an interactive segmentation and where user interaction can be applied. The major assumption for this interaction process is that the user who is interacting should have a correct and clear vision of the desired segmentation result. The user should also be able to judge what types of dedicated segmentation algorithms are needed. Guiding the segmentation algorithm to find and improve correct segmentation results in an efficient way is also the user's role in the interactive segmentation process.

In an interactive scenario, the purpose of the user interaction can be summarized in the following ways:

1. To judge whether the segmentation result is correct.

2. To choose a function/option to perform a dedicated segmentation algorithm.

3. To initialize a starting position on the image for the segmentation algorithm.

4. To set/change parameter values for the segmentation algorithm.

5. To compose/modify the primitive results obtained from a segmentation algorithm.

Combinations of these purposes in user interaction can be found in several previous works [16, 42, 71, 50, 10]. Ideally, an effective and efficient interactive segmentation system should serve as much a combination of the purposes described above as possible, i.e., a simple mouse click can both judge whether the result obtained is correct and to choose a segmentation algorithm to perform the task.

5.2 Types of User Interaction

Besides the purposes of user interaction, we should also be aware of the common existing types of interaction between the user and the computer in image processing. These common types of user interaction exist in tasks such as image segmentation, image editing, image post-processing, etc. A good interactive system should design simple and effective interactions which require minimal user input. One way of categorizing the types of user interaction in image segmentation are listed as following:

1. **Point.** For example, a single mouse click or multiple clicks to add or delete seeds in segmentation algorithms such as snake and active contour models [42].

2. **Line.** For example, a stroke to specify labeling pixels for foreground or background in the graph cut algorithm [16].

3. **Area.** For example, a couple of clicks to specify the region of interest in the grabcut algorithm [71].

4. **Volume.** For example, for three-dimensional structure segmentation, multiple mouse clicks can define the volume of interest.

5.3 Common Segmentation Mistakes

Segmentation algorithms fail when the object in the image deviates too much from the ideal appearance covered by the segmentation model [66]. On the other hand, it is important to note that, in a lot of cases, segmentation mistakes are still confined to part of the desired object of interest. Based on this observation, in this chapter, we will develop a comprehensive interactive image segmentation framework based on common segmentation mistakes. We observe that there are a finite number of cases of failure, which correspond to the finite number of tools needed in the interactive segmentation system. To sum up, most existing segmentation algorithms are bounded to fail in the following situations:

1. When an object of interest should be segmented but is missing, an **addition** action is needed to add such an object.

2. When an object should not be there but is included in the segmentation result, a **deletion** action is needed to remove it.

3. When the segmentation algorithm under-segments the objects due to object fusion, a **splitting** action is needed to split two or more than two connected components.

4. When the segmentation algorithm over-segments the object of interest into multiple objects, a **merging** action is needed to merge two or more disconnected objects.

5. When the visual evidence is too low, or there is too much noise from the image, or there is misleading visual evidence, etc., a **boundary refinement** action is needed to refine/edit the incorrectly segmented portions of the object.

Although there are no universal rules of the types of mistakes of all possible segmentation algorithms, from observations, most segmentation algorithms are bounded to make similar mistakes as stated above. Interestingly, **splitting** and **deletion** actions deal with under-segmentation misktaes, while **merging** and **addition** actions deal with over-segmentation mistakes. **Boundary refinement** can deal with both under- and over-segmentation.

5.4 An Interactive Segmentation System based on Common Segmentation Mistakes

In an interactive segmentation system, the interactive tools available to the user must be powerful and intuitive, and allow efficient interaction. Depending on the purpose of user interaction, the corresponding tool should be specific for the action that the user wants to perform. It is inefficient to design one universal editing tool as it will display nonspecific performance, because each of the mistakes described in Section 5.3 leads to a different type of algorithm or method.

Since we have concluded that there are commonly five types of segmentation mistakes, subsequently, five types of tools are needed to deal with each of the mistakes: addition, deletion, splitting, merging and boundary refinement. For each interactive tool, a corresponding method will be designated. Table

5.1 gives a summary of the different types of segmentation mistakes and the corresponding actions proposed. Figure 5.1 presents a general flowchart of our proposed interactive image segmentation system.

Table 5.1: Interactive tools, the corresponding reasons for the tools and detailed actions for the tools in the proposed interactive segmentation system

Tools	**Reasons**	**Actions**
Addition	Object of interest is missing	Add an object of interest
Deletion	Segmented object should be removed	Remove an object
Splitting	Under-segmentation	Split one object into two, or more than two, objects
Merging	Over-segmentation	Merge two, or more than two, disconnected objects
Boundary Refinement	Visual evidence is low, misleading visual evidence, etc.	Refine the boundary to a more desired segmentation

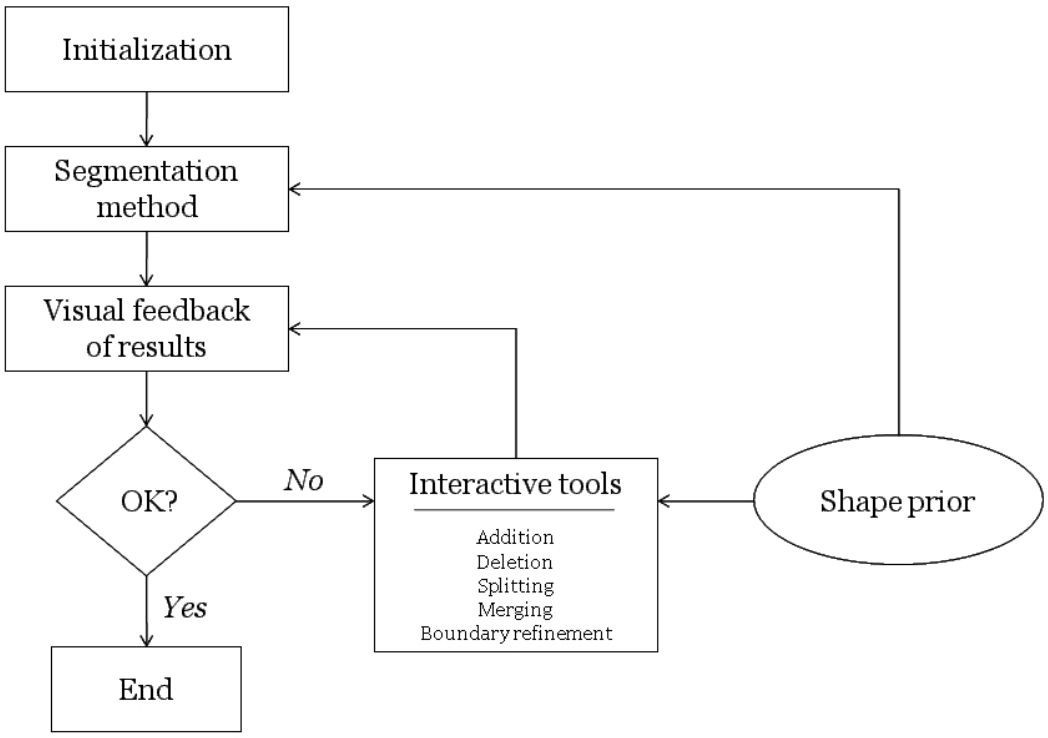

Figure 5.1: The general flowchart of our proposed interactive image segmentation system.

For each of the five cases in the proposed framework, we apply either one of the shape-guided algorithms we described in the previous chapters, or an interactive method. For addition, the adaptive shape prior method described in Chapter 2 can be utilized. For deletion, the user can interactively select each unwanted object or a whole region in which unwanted objects are. For splitting, the clump splitting method via bottleneck detection described in Chapter 3 can be applied. For merging, we design an interactive way to let the user select adjacent objects to be merged by joining the touching boundaries between them. Finally, boundary refinement can be achieved by the shape PCA method presented in Chapter 4.

Table 5.2 provides a summary of each of the interactive tools and their corresponding methods described in this dissertation. The proposed framework is an example to integrate all the proposed shape-guided algorithms in this dissertation. On the other hand, this proposed system is not constrained by these shape-guided segmentation algorithms. It is flexible and should easily integrate other types of segmentation algorithms.

Table 5.2: Summary of the interactive tools and their corresponding methods for the proposed interactive segmentation system

Tools	**Methods**
Addition	Adaptive Shape Prior
Deletion	Interactive Object Deletion
Splitting	Clump Splitting via Bottleneck Detection
Merging	Interactive Objects Merging
Boundary Refinement	Shape PCA

5.5 Experimental Results

This section presents the details of the proposed interactive segmentation system and the extensive experimental evaluation of the system, focusing on the

image segmentation performance and the system usability study. The segmentation performance is evaluated both quantitatively and visually, and the usability study is performed in terms of action per object.

5.5.1 Experiment Details

5.5.1.1 System Interface

The proposed interactive segmentation system has been designed and implemented. Figure 5.2 on page 92 shows an example of the user interface developed as an illustration of how this system works, in which an example on oil sand image segmentation is displayed. In this example, once the user selects to open an input image from (1), the selected image will be loaded and displayed in the image window at (2) on the user interface. To obtain the initial segmentation result for this image, the user can either choose an existing segmentation algorithm among the methods listed in (3), or select an image of the saved segmentation result from previous work from (1). In this example, the four segmentation algorithms listed in (3) are examples of segmentation algorithms we applied in our experiments for generating the initial segmentation results. Once the initial segmentation result of the selected image is obtained, this result is displayed in *green* boundaries of the segmented objects on top of the original image, as shown in Figure 5.2.

When the user starts to visually judge the initial segmentation results, the system provides different ways for the user to interactively select the desired segmentation tools. To begin with, there are some basic image processing tools available listed in (4), based on the users' feedback. These tools include some automatic image post-processing functions such as filling holes, shape filters, etc. Furthermore, the five major interactive tools proposed in this system are available at position (6) to (10). By selecting these tools, the user can easily choose any of the five proposed interactive tools at any stage of the

segmentation. For each of the five tools, there are also choices for different levels of user interaction. For example, for addition displayed at (6), the user can select between ASP, livewire, or simply tracing the boundary manually. For deletion tool at position (7), the user can select either one object to delete by clicking on the unwanted object, or a region of interests to delete all the objects within the region by two mouse clicks. For splitting and merging, we set the default number of objects to be two. For boundary refinement at (10), the user can also select between Shape PCA, ASP and livewire.

Besides image segmentation, there are also some practical functions implemented such as viewing only raw image or segmented results at (13), generating segmentation evaluation for the purpose of collecting segmentation results at (5), undo and redo buttons at (11), and freeze or unfreeze an object at (12) so that the user cannot modify it anymore. All these functions together fulfill the practical purpose of this system.

5.5.1.2 Test Data Set

To establish whether the proposed system in this chapter indeed has merit, we have carried out extensive experiments on two challenging data sets: oil sand images from mining industry and leukocyte microscopy images from medical imaging. Oil sand mining images were captured as a part of the performance evaluation of an oil sand crusher [100, 1] and leukocyte images were captured as a part of inflammation study [3].

Oil sand images are a very challenging data set because the image quality is limited by acquisition. A big amount of research has been done on accurately segmenting oil sand images [53, 65, 74, 77, 98, 88, 87, 89]. From experience and experiments, image level information provided is far from enough to obtain accurate segmentation for this type of images. On the other hand, shape feature is one of the most distinguished features in oil sand images [65, 76].

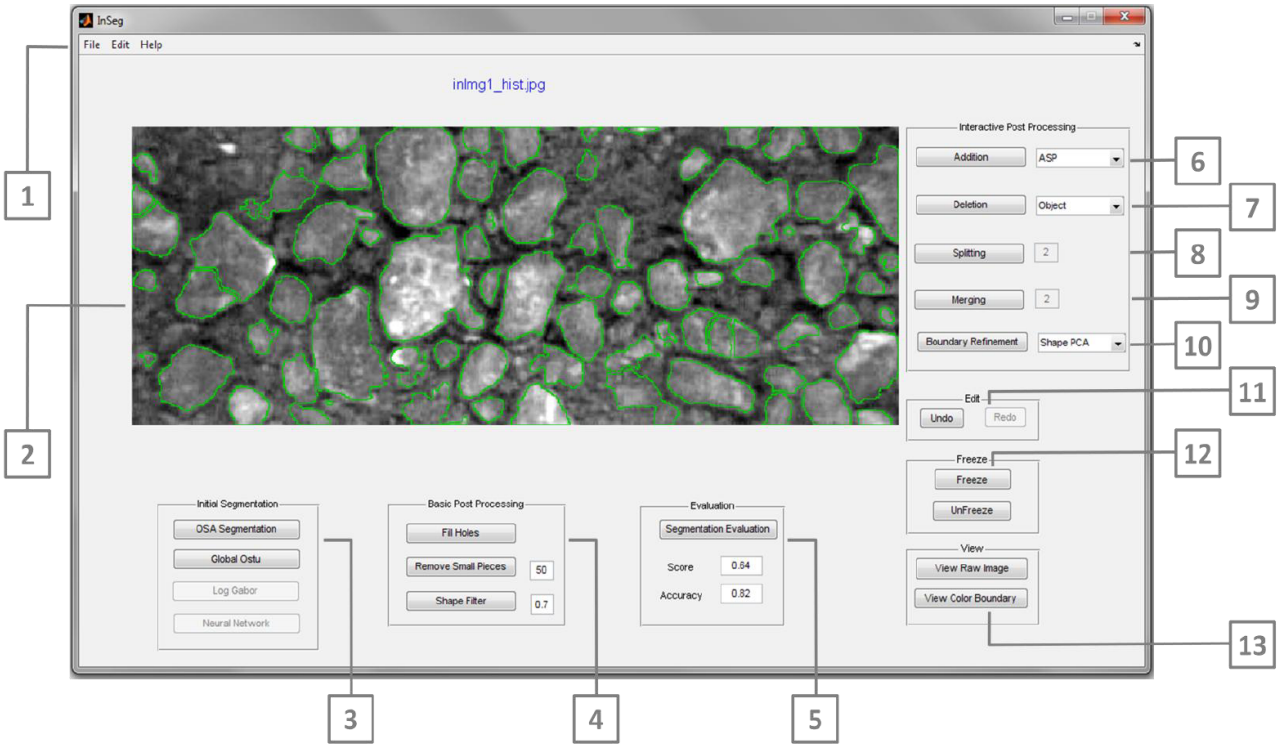

1	Menu
2	Basic Post Processing Methods
3	Display Window
4	Initial Segmentation Methods
5	Segmentation Evaluation
6	Interactive Segmentation Tools – Addition
7	Interactive Segmentation Tools – Deletion
8	Interactive Segmentation Tools – Splitting
9	Interactive Segmentation Tools – Merging
10	Interactive Segmentation Tools - Boundary Refinement
11	Undo/redo Buttons
12	Freeze/unfreeze Buttons
13	Display Options

Figure 5.2: An example of the user interface for the proposed interactive segmentation system. This example demonstrates the segmentation of an oil sand image with the initial segmentation results displayed in *green* boundaries of the segmented objects on top of the original input oil sand image.

Furthermore, to demonstrate the general applicability of this research, we have also applied our interactive segmentation system on the leukocyte images. Leukocyte plays an important role in the study of inflammation [3]. Typical leukocyte studies on leukocyte images require segmenting and tracking leukocyte. Several challenges exist in automatic delineation of leukocyte microscopy images, which are described in [73].

5.5.2 Segmentation Evaluation

Different experiments were performed on both oil sand images and leukocyte images to evaluate the segmentation improvement. We carried out experiments of both performing all tools on the images, and performing only one tool on the images each time. Image segmentation performance is usually evaluated both quantitatively and visually. Although visual evaluation by humans is very intuitive and straightforward, it is sometimes subjective. Quantitative evaluation is on the other hand more objective. In both data sets, manual segmentation results from experts are defined as our ground truth images. In our evaluation, we compute the difference between the ground truth and the segmentation result using evaluation metric such as pixel accuracy and object score. The rest of this section describes the details of each of the experiments and the corresponding evaluation results visually and quantitatively.

Experiment 1: applying the complete system to oil sand images

In this experiment, the complete interactive system of all five tools is applied when necessary to the oil sand images. We choose this group of images because they are the same data set studied thoroughly in the previous work on oil sand image segmentation [53, 54].

In this experiment, we have applied four types of different segmentation algorithms to generate the initial segmentation results, as a starting point of

the test data set. This is to test whether our system is dependent on a certain type of segmentation algorithm. The four initial types of segmentation algorithms are a deep neural network based method (NN) from [53], ground truth decomposition method via Gabor filter (logGabor) from [54], OSA method (OSA) [4] and Otsu's method (Otsu) [68].

An example of the visual results is shown in Figure 5.3 which demonstrates the segmentation improvement visually. It shows the original oil sand image in (a), the corresponding initial segmentation result from a neural network based segmentation algorithm (NN) [53] in (b) and the final result after applying our segmentation system on (b) in (c). We can see that with the help of the five tools, the segmentation quality has been significantly improved in the final result.

Table 5.3 and Table 5.4 show the quantitative results on the improvement of pixel accuracy and object score respectively, after applying our complete system to the test data set of oil sand images. From both accuracy and score improvement, it is clear that the proposed system has improved the segmentation quality on both pixel and object level. Since each of the initial segmentation results obtained from the four different segmentation algorithms has obtained segmentation improvements by using our system, this shows that the improvement from our system is independent of the initial segmentation algorithm. Furthermore, it is also interesting to see that a segmentation algorithm which performs worse initially, such as OSA or logGabor method, benefits more from the system in terms of accuracy and score improvement. This is because such a method makes more mistakes in the initial segmentation stage and thus provides the system with more opportunities to improve.

In addition, when comparing the pixel accuracy improvement with the object score improvement, the quantitative improvement on the object scores is in general higher than the pixel level accuracies. This is because the object

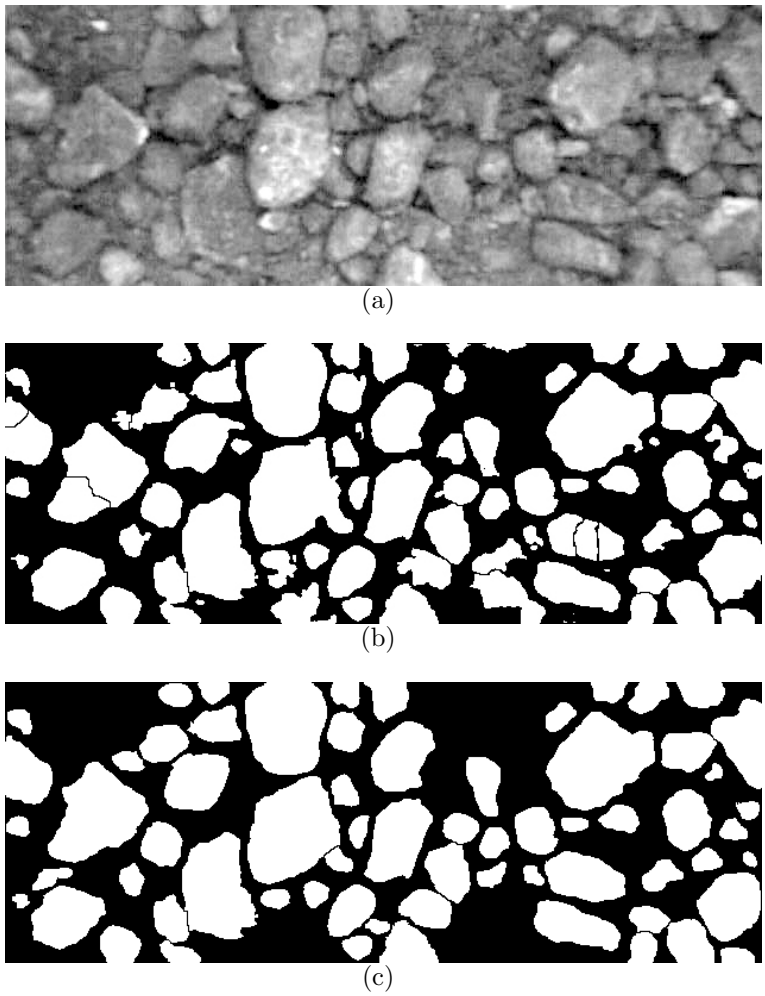

Figure 5.3: An example of the visual results on oil sand image to compare the original image (a), the corresponding initial segmentation result from [53] (b) and the final result (c).

level score takes into account and penalizes under- and over-segmentation more than pixel level accuracy [70]. Since tools such as splitting and merging target at under- and over-segmentation problems, the segmentation improvement on the object level could be significant while the improvement on pixel accuracy level could be subtle.

Experiment 2: applying each of the five tools independently to oil sand images

Besides applying the complete system to oil sand images, each of the five tools

Table 5.3: Accuracy improvement on oil sand images for the complete system with four different kinds of initial segmentation algorithms

Method	**accuracy before**	**accuracy after**	**diff**
NN	0.84	0.86	0.02
logGabor	0.75	0.79	0.03
OSA	0.72	0.78	0.06
Otsu	0.76	0.79	0.03

Table 5.4: Score improvement on oil sand images for the complete system with four different kind of initial segmentation algorithms

Method	**score before**	**score after**	**diff**
NN	0.67	0.72	0.05
logGabor	0.43	0.56	0.13
OSA	0.47	0.57	0.10
Otsu	0.48	0.57	0.08

is also applied independently to each of the oil sand images to demonstrate and compare the effectiveness of each tool. In this experiment, we allow the user to apply only one of the five tools from the system on the image repeatedly until no more improvement is possible. Then, the pixel accuracy and object score improvement made by each of the five tools are recorded and compared. This experiment is performed on the same set of images as in Experiment 1. The NN method [53] is chosen to be the initial segmentation algorithm due to its superior performance over the other methods on oil sand images.

Accuracy improvement made by each of the tools is demonstrated in Figure 5.4 and score improvement is presented in Figure 5.5. From the object score improvement, it is clear that tools such as addition, deletion, splitting and merging improve the segmentation more than boundary refinement. This is expected because boundary refinement only focuses on improving the shape of the final segmentation boundary, which can be very subtle when it is evaluated in both pixel level accuracy and object level score. Furthermore, addition

improves both accuracy and score the most due to the fact that adding an object affects the total number of pixels and objects more than the other tools.

Another interesting observation is that simply combining the improvement made by all the tools does not equal to the overall improvement made by the complete system described in Experiment 1. This is because that some of the segmentation improvements should be made when combining two or more than two of the tools in the system, instead of only applying one of the tools. For example, an under-segmented clump might need to be split first, then some of the objects that result from the split should be merged with some other objects to obtain the final result.

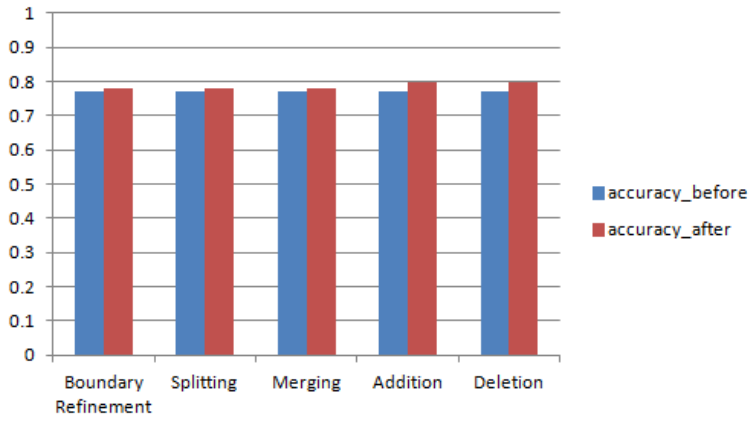

Figure 5.4: Improvement on pixel accuracy generated by each of the five tools for oil sand images

Experiment 3: applying the complete system to leukocyte images

To further demonstrate the general applicability of the proposed system, similar to Experiment 1, the system was also applied to the segmentation of leukocyte images. The same procedure in Experiment 1 is followed for applying all necessary tools of the complete system to leukocyte images. The leukocyte image data set consists of nine images from a previous study in [73].

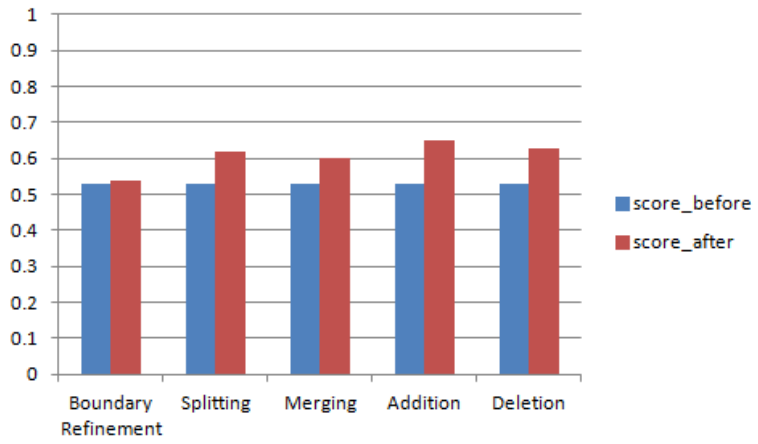

Figure 5.5: Improvement on object score generated by each of the five tools for oil sand images

The initial segmentation of the images was obtained from boosting method in [73].

An example of the visual results are shown in Figure 5.6 to demonstrate the improvement from our system visually. It shows the original leukocyte image in (a), the corresponding initial segmentation result from [73] in (b) and the final result after applying our system on (b) in (c). We can see that the segmentation quality has been improved significantly in (c).

Table 5.5 shows the quantitative results on accuracy and score improvement on leukocyte images respectively. The accuracy and score beforehand come from the segmentation by a snake based boosting method [73], and the accuracy and score afterwards come from the final results after applying our system. Similar to the results in oil sand images, the quantitative improvement on the object score is tremendous while the improvement on pixel accuracy is relatively subtle. This is also because plitting and merging are the most needed tools when improving the segmentation for leukocyte images, and these improvements are generally reflected more when evaluated by object score since object score penalizes under- and over-segmentation more than pixel accuracy.

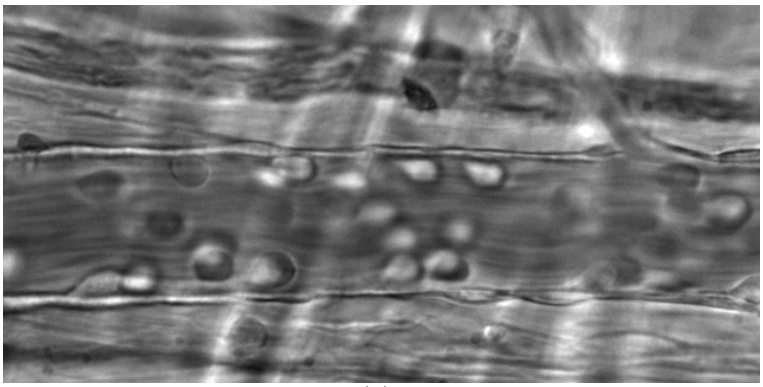

(a)

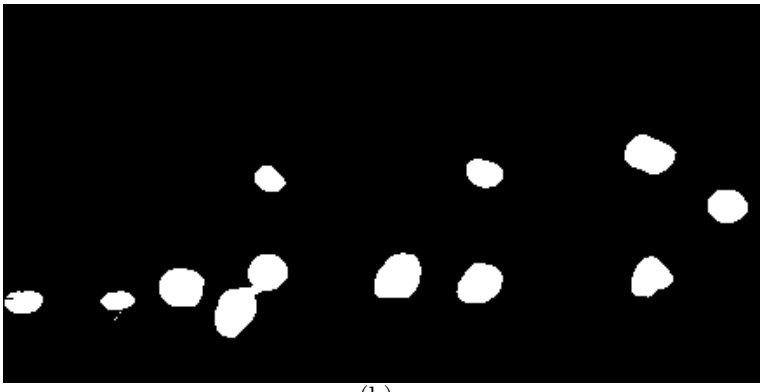

(b)

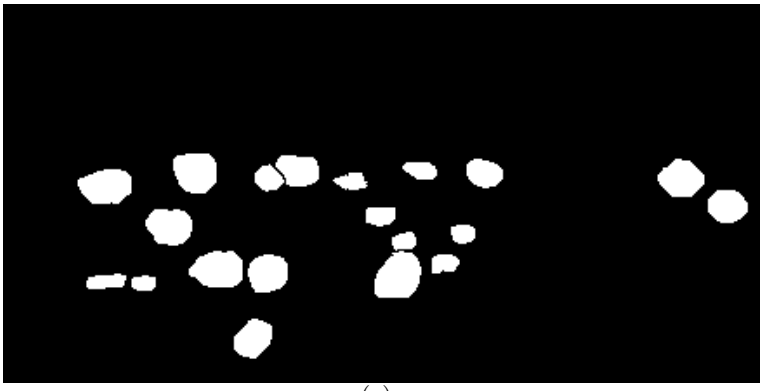

(c)

Figure 5.6: An example of the visual results on leukocyte image to compare the original image (a), the corresponding initial segmentation result from [73] (b) and the final result (c).

Experiment 4: applying each of the five tools independently to leukocyte images

Similar to Experiment 2, besides applying the complete system to leukocyte images, each of the five tools is also applied independently to leukocyte images

Table 5.5: Accuracy and score improvement on leukocyte images for the complete system

accuracy before	**accuracy after**	**diff**
0.95	0.98	0.03
score before	**score after**	**diff**
0.51	0.67	0.16

to demonstrate and compare the effectiveness of each tool. This experiment is performed on the same set of images as in Experiment 3.

Improvement made by each of the tools is demonstrated in Figure 5.7 for pixel accuracy and Figure 5.8 for object score. Both figures show that addition, deletion and splitting improve the segmentation more than the other tools. Especially from Figure 5.8, it is clear that addition and splitting have improved the object level score the most.

In addition, when comparing the results from Experiment 4 to results from Experiment 2, it is also interesting to notice that the performance on each of the five tools is application dependent. Since different applications encounter different segmentation mistakes, each of the five tools can be either applied independently or combined together to achieve the best improvement for the specific application.

5.5.3 Usability Study

Usability study is an important step for an interactive segmentation system. Various ways of usability studies exist for interactive segmentation algorithms. Lazy snapping [56] conducts its usability study based on criteria such as ease of use, time spent and user feedback. For evaluating selection accuracy over time, edge-respecting brushes method [67] studies user experience by giving the users a specific amount of time, instructing them to achieve as much accuracy as possible within that time and then comparing the user's results to average

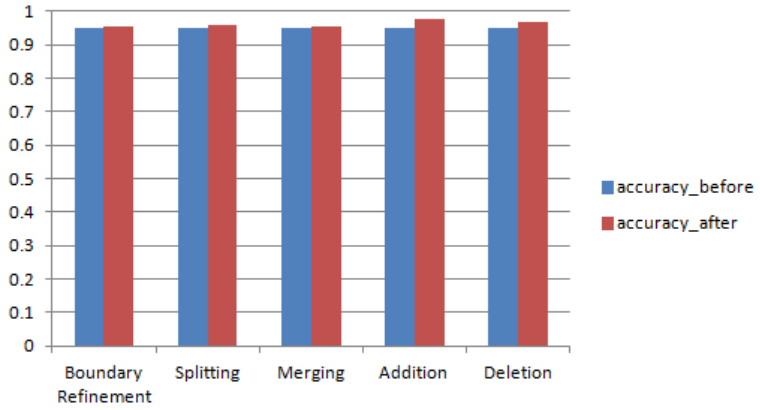

Figure 5.7: Improvement on pixel accuracy generated by each of the five tools for leukocyte images

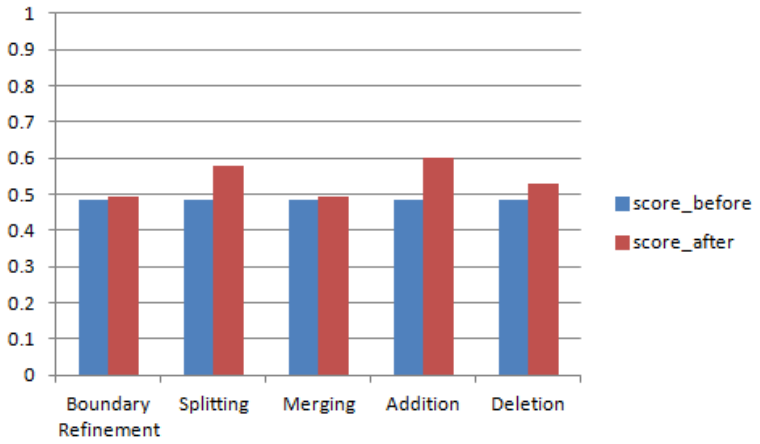

Figure 5.8: Improvement on object score generated by each of the five tools for leukocyte images

ground truth results. To evaluate the usability and efficiency of our proposed interactive system, we did the following evaluations in quantitative measures, which are common usability measures that exist in the literature.

Experiment 5: Action per object

To evaluate the amount of user interaction needed from the user, we have performed a usability study to record the total number of objects per image and the total number of actions (mouse clicks) performed by the user. The

users have applied the complete system to both oil sand images and leukocyte images. When the segmentation task is finished, the total number of actions was recorded. For oil sand image segmentation, the same four segmentation algorithms (NN, logGabor, OSA, Otsu) from Experiment 1 were utilized as the initial segmentation algorithms. The initial segmentation of leukocyte image was from [73] as in Experiment 3 and 4.

Figure 5.9 demonstrates the action per object rate of our system for each of the initial segmentations generated by the segmentation algorithms listed. We can see that depending on the quality of the initial segmentation, the number of actions needed for each object varies between 0.55 to 1.45. This means that for each object in the image, the user needs around one to three clicks per two objects, which is highly efficient compared to stroke based methods such as graph cut and boundary tracing methods such as livewire.

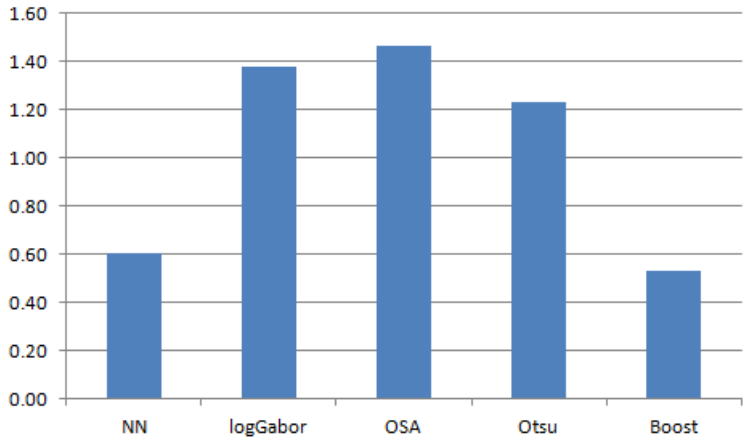

Figure 5.9: Usability study on the proposed segmentation system in terms of action per object, i.e., the total number of mouse clicks each object needs in the images. NN, logGabor, OSA and Otsu represent that the initial segmentation is obtained from a neural network based method [53], a ground truth decomposition method via Gabor filter [54], the OSA method [4], and Otsu's method [68] for oil sand images, respectively. Boost represents that the initial segmentation for leukocyte images are obtained from a boosting method [73].

5.6 Summary

The chapter has proposed a novel and comprehensive interactive image segmentation system as an example to integrate the proposed shape-guided algorithms in the previous chapters. This proposed segmentation system is developed based on the observation that common cases of failure from segmentation algorithms can be categorized in five basic types, each of which needs a corresponding segmentation algorithm. Therefore, five different decisive tools which intuitively reflect user's intention are developed: addition, deletion, splitting, merging and boundary refinement. From observation, most image segmentation tasks can be handled by one or a combination of these five tools.

By combining them, a state-of-the-art shape-guided interactive segmentation system can be constructed which is capable of extracting high quality foreground objects from an image effectively and efficiently with only one or two mouse clicks per object. Experimental results from both segmentation quality evaluation and user study have shown the effectiveness and efficiency of this system.

Chapter 6

Conclusions

6.1 Conclusions

This dissertation focuses on improving image segmentation with the combination of shape-guided segmentation algorithms and minimal user interaction. Starting with an image, the initial segmentation is achieved with some segmentation algorithms. Then, to deal with certain types of under- and over-segmentation mistakes, clump splitting and merging are required on top of the initial segmentation. Finally, boundary refinement is needed to finalize the shape of the segmentation results. For each types of different interactive segmentation, shape information is utilized to guide the segmentation algorithms.

The segmentation can be first achieved by the proposed adaptive shape prior method (ASP) in the graph cut framework. The ASP method is proposed to incorporate shape priors adaptively, depending on the need of the shape prior at each pixel on the image. The ASP method eliminates mistakes from previous approaches in which parameters had to be tuned to fit the image. It works by adding the shape term in the energy function based on a probability map, which can be obtained by, for example, image enhancement and is therefore straightforward, automatic and with little extra computational cost to the algorithm. We have shown that ASP can be easily applied to various types of graph cut based segmentation algorithms with shape priors, such as shape template and star shape method.

To deal with under-segmentation such as clump splitting, the bottleneck detection method is proposed to take advantage of shape information on the bottleneck of a clump. The proposed method consists of three steps and has several advantages over existing methods. First, our method is not parameter-dependent on finding candidate points for splitting, unlike most existing methods, especially concavity based methods, which are highly parameter-dependent.

Second, our method avoids dealing with special situations in which the splitting points are not concave, in which almost all existing methods need to add extra points according to the heuristic rules and constraints. Furthermore, our method takes intensity information into account in localizing the cut between splitting points and finds a more accurate cut than the straight-line cut that directly joins the splitting points. Finally, the proposed shape classification method determines the number of splits for each clump, which is more flexible than model based methods.

Subsequently, in order to refine the incorrectly segmented portions of the object boundary obtained from previous steps, the shape PCA method is developed to utilize statistical shape information when image level information is inadequate or missing. The shape PCA method takes advantage of shape information which is not directly available from image level and improves the object boundary using the first few selected principal components which presumably represents the true shape of the object. A local shape PCA method is also proposed in contrast to the global shape PCA method. As long as the incorrectly segmented portions of the object boundary can be localized correctly, either automatically or manually, local shape PCA can be easily applied to perform boundary refinement.

Finally, as an example to integrate these proposed shape-guided algorithms together, a comprehensive interactive segmentation system is developed which is composed of five different decisive tools that intuitively reflect the intention of the user: addition, deletion, splitting, merging and boundary refinement. From observations, most image segmentation tasks can be handled by one or a combination of these five tools. Specifically, the user interaction takes place in a scenario where the segmentation results are progressively refined by a combination of the shape-guided methods proposed in this dissertation. By combining them, a state-of-the-art shape-guided interactive segmentation sys-

tem can be constructed which is capable of extracting high quality foreground objects from images effectively and efficiently with minimal amount of user input.

6.2 Future Work

The potential future research for shape-guided interactive segmentation can be identified as follows:

- Incorporating the adaptive shape prior into energy functions other than graph cut. So far we have proposed and successfully incorporated shape priors adaptively into the graph cut based energy functions. While graph cut is one of the most successful interactive segmentation algorithms in recent decades, other types of energy functions based on level set are also widely used in automatic image segmentation. Further research are needed to determine the generality and capability of the adaptive shape prior idea, e.g., if it is possible to incorporate this idea into level set based energy functions. Another direction is to examine whether more types of shapes can be incorporated into the adaptive shape prior segmentation framework, either graph cut or level set based framework. While we have seen that the current method is relatively robust compared to other existing shape prior methods, it will be interesting to see whether this robustness holds in the case of greater variations in shapes and images, and if not, how the algorithm maybe modified to account for these changes.

- Selecting the number of principal components for the shape PCA method adaptively. Currently, the number of principal components selected in the shape PCA method is determined based on our observation and experience from the experiments for certain types of applications. How-

ever, we notice that ideally, for different types of image applications with different shapes, there will be different number of principal components needed to perform the shape PCA method and achieve the best result. Even for different objects within the same application, the need for the number of principal components might also vary because some object shapes are better segmented in the initial segmentation than others. Therefore, we would like to explore the possibility of determining the number of principal components needed for obtaining the true shape of the object more adaptively.

- Interactive merging. So far the proposed interactive merging method developed in our interactive segmentation system is a simple and straightforward method which only works for merging adjacent objects that touch each other. Our method simply eliminates the touching boundary of the objects and merges the selected pieces into one. In the future work, we would like to explore possible shape-guided segmentation algorithms to not only find the merging boundary of the objects under some shape guidance, but also merge objects which are not directly adjacent to each other.

- Applying reinforcement learning (RL) to the proposed segmentation system. Based on the observation that similar mistakes are often made repetitively in the same application and the same interactive tool is often selected for such type of mistakes to perform the segmentation, applying RL to incrementally learn and eventually automate this interactive procedure is a natural continuation of this PhD dissertation. The RL applied to this proposed segmentation system should learn from the user interaction incrementally, and eventually performs the selection of the tools with little need of user interaction. RL has the nature of learning

both offline and online, and can continuously learn and adapt to the updated environment while the user performs the task. This is useful in an interactive segmentation task.

Bibliography

[1] Issue: Canadians want responsible development of the oil sand, 2007. Sustainability Report.

[2] Image matting. http://www.computervisiononline.com/node/238, January 2012. Internet access.

[3] Inflammation: The leukocyte adhesion cascade. http://bme.virginia.edu/ley, January 2012. Internet access.

[4] OSA. http://webdocs.cs.ualberta.ca/ cims/research/projects.html, January 2012. Internet access.

[5] Agilent Technologies Inc. Post processing pico image software for agilent afm systems. Internet: cp.literature.agilent.com/litweb/pdf/5989-7596EN.pdf, November 2007. Datasheet.

[6] S. Araki, N. Yokoya, H. Iwasa, and H. Takemura. A new splitting active contour model based on crossing detection. In *Proceedings of the Second Asian Conference on Computer Vision*, volume II, pages 346–350, 1995.

[7] S. Avidan and A. Shamir. Seam carving for content-aware image resizing. *ACM Transactions on Graphics*, 26(3):10, 2007.

[8] X. Bai, C. Sun, and F. Zhou. Splitting touching cells based on concave points and ellipse fitting. *Pattern Recognition*, 42(11):2434–2446, 2009.

[9] I. Bar-Yosef, A. Mokeichev, K. Kedem, I. Dinstein, and U. Ehrlich. Adaptive shape prior for recognition and variational segmentation of degraded historical characters. In *Pattern Recognition*, volume 42, pages 3348–3354, 2009.

[10] W. A. Barrett and A. S. Cheney. Object-based image editing. In *29th Annual Conference on Computer Graphics and Interactive Technique*, pages 777–784, 2002.

[11] O. Basset and C. Cachard. Ultrasound image post-processing - application to segmentation. *Physics for medical imaging applications*, 240:227–239, 2007.

[12] A. C. Berg. *Shape Matching and Object Recognition*. PhD thesis, U. C. Berkeley, December 2005.

[13] S. Beucher and C. Lantuejoul. Use of watersheds in contour detection. In *Proceedings of the International Worksscla hop on Image Processing, Real-Time Edge and Motion Detection/Estimation*, pages 17–21, 1979.

[14] A. Blake, C. Rother, M. Brown, P. Perez, and P. Torr. Interactive image segmentation using an adaptive GMMRF model. In *Proceedings of the European Conference in Computer Vision*, pages 428–441, 2004.

[15] F. L. Boostein. Landmark methods for forms without landmarks: localizing group differences in outline shape. *Medical Image Analysis*, 1(3):225–244, 1997.

[16] Y. Y. Boykov and M.-P. Jolly. Interactive graph cuts for optimal boundary and region segmentation of objects in N-D images. In *Proceedings Eighth IEEE International Conference on Computer Vision*, volume 1, pages 105–112, 2001.

[17] C. C. Chang and C. J. Lin. LIBSVM: A library for support vector machines. Internet: www.csie.ntu.edu.tw/ cjlin/libsvm, 2011. Software.

[18] T. Cootes and C. Taylor. Statistical models of appearance for computer vision, February 2012. Internet access.

[19] T. F. Cootes, G. J. Edwards, and C. J. Taylor. Active appearance models. In *Proceedings of the 5th European Conference on Computer Vision*, volume 2, pages 484–498, 1998.

[20] T. F. Cootes, G. J. Edwards, and C. J. Taylor. Active appearance models. *IEEE Trans. on Pattern Analysis and Machine Intelligence*, 2001.

[21] T. F. Cootes and C. J. Taylor. Statistical models of appearance for computer vision. Internet: http://www.isbe.man.ac.uk/ bim/,, October 2001. Technical Resport.

[22] T. F. Cootes, C. J. Taylor, D. H. Cooper, and J. Graham. Training models of shape from sets of examples. In *British Machine Vision Conference*, pages 9–18, 1992.

[23] T. F. Cootes, C. J. Taylor, D. H. Cooper, and J. Graham. Active shape models - their training and application. *Computer Vision and Image Understanding*, 61:38–59, 1995.

[24] D. Cremers, T. Kohlberger, and C. Schnorr. Nonlinear shape statistics in mumford-shah based segmentation. In *IEEE European Conference on Computer Vision*, pages 93–108, 2002.

[25] P. Das, O. Veskler, V. Zavadsky, and Y. Boykov. Semiautomatic segmentation with compact shape prior. In *Image and Vision Computing*, volume 27, pages 206–219, 2009.

[26] E. W. Dijkstra. A note on two problems in connexion with graphs. *Numerische Mathematik*, 1:269–271, 1959.

[27] I. L. Dryden and K. V. Mardia. *Statistical Shape Analysis*. John Wiley & Sons, Chichester, 1 edition, September 1998.

[28] N. Duta, A. K. Jain, and M.-P. Dubuisson-Jolly. Learning 2d shape models. In *Proceedings Conf. on Computer Vision and Pattern Recognition*, volume 2, pages 8–14, 1999.

[29] M. Farhan. Automated clump splitting for biological cell segmentation in microscopy using image analysis. Master's thesis, Tampere University of Technology, Finland, November 2009.

[30] M. Farhan, O. Yli-Harja, and A. Niemisto. An improved clump splitting method for convex objects. In *International Workshop on Computational Systems Biology*, pages 35–38, 2010.

[31] G. Fernandez, M. Kunt, and J.-P. Zryd. A new plant cell image segmentation algorithm. In *International Conference of Image Analysis and Processing*, pages 229–234, 1995.

[32] D. Freedman and T. Zhang. Interactive graph cut based segmentation with shape priors. In *Computer Vision and Pattern Recognition*, pages 755–762, 2005.

[33] R. C. Gonzalez and R. E. Woods. *Digital Image Processing*. Prentice Hall, 2 edition, January 2002.

[34] O. Gormeza and H. H. Yilmazb. Image post-processing in dental practice. *European Journal of Dentistry*, 3(4):343–347, October 2009.

[35] X. C. He and N. H. C. Yung. An efficient segmentation algorithm based on mathematical morphology and improved watershed. *Intelligent Computing in Signal Processing and Pattern Recognition*, 345:689–695, 2006.

[36] F. Heckel, O. Konrad, H. K. Hahn, and H.-O. Peitgen. Interactive 3d medical image segmentation with energy-minimizing implicit functions. *Computers & Graphics*.

[37] T. Heimann and H.-P. Meinzer. Statistical shape models for 3d medical image segmentation: A review. *Leitfaden der angewandten Informatik*.

[38] D. M. Hobson, R. M. Carter, and Y. Yan. Rule based concave curvature segmentation for touching rice grains in binary digital images. In *IEEE Instrumentation and Measurement Technology Conference*, pages 1685–1689, May 2009.

[39] H. Ip and R. Yu. Recursive splitting of active contours in multiple clump segmentation. *Electronics Letters*, 32(17):1564–1566, August 1996.

[40] P. Jaccard. étude comparative de la distribution florale dans une portion des alpes et des jura. *Bulletin del la Société Vaudoise des Sciences Naturelles*, 37:547–579, 1901.

[41] V. Jain and H. S. Seung. Natural image denoising with convolutional networks. In *Advanceds in Neural Information Processing Systems*, 2008.

[42] M. Kass, A. Witkin, and D. Terzopoulos. Snakes: Active contour models. *International Journal on Computer Vision*, 1(4):321–331, 1987.

[43] V. Kindratenko. *Development and Application of Image Analysis Techniques for Identification and Classification of Microscopic Particles*. PhD thesis, University of Antwerp, Belgium, 1997.

[44] M. Kirby. *Geometric Data nalysis: An Empirical Approach to Dimensionality Reduction and the Study of Patterns*. John Wiley & Sons, New York, 2001.

[45] V. Kolmogorov and R. Zabih. Multi-camera scene reconstruction via graph cuts. In *European Conference on Computer Vision*, pages 82–96, 2002.

[46] V. Kolmogorov and R. Zabih. What energy functions can be minimized via graph cuts. *IEEE Transactions on Pattern Analysis and Machine Intelligence*, 26(2):65–81, 2004.

[47] M. Kumar, P. Torr, and A. Zisserman. Obj cut. In *IEEE Conference on Computer Vision and Pattern Recognition*, pages 18–25, 2005.

[48] S. Kumar, S. H. Ong, S. Ranganath, T. C. Ong, and F. T. Chew. A rule-based approach for robust clump splitting. *Pattern Recognition*, 39(6):1088–1098, June 2006.

[49] E. G. Learned-Miller. Data driven image models through continuous joint alignment. In *IEEE Transactions on Pattern Analysis and Machine Intelligence*, volume 28, 2006.

[50] V. Lempitsky, P. Kohli, C. Rother, and T. Sharp. Image segmentation with a bounding box prior. In *IEEE International Conference on Computer Vision*, pages 277–284, 2009.

[51] A. Levin, D. Lischinski, and Y. Weiss. A closed-form solution to natural image matting. *IEEE Transactions on Pattern Analysis and Machine Intelligence*, 30:228–242, 2008.

[52] A. Levin, A. Rav-Acha, and D. Lischinski. Spectral matting. In *IEEE Transactions on Pattern Analysis and Machine Intelligence*, volume 30, pages 1699–1712, 2008.

[53] I. Levner. *Data Driven Object Segmentation*. PhD thesis, Department of Computing Science, University of Alberta, 2008.

[54] I. Levner, R. Greiner, and H. Zhang. Supervised image segmentation via ground truth decomposition. In *IEEE International Conference on Image Processing*, pages 737–740, 2008.

[55] Y. Li, J. Sun, and H.-Y. Shum. Video object cut and paste. In *SIGGRAPH 2005*, pages 595–600, 2004.

[56] Y. Li, J. Sun, C.-K. Tang, and H.-Y. Shum. Lazy snapping. In *SIGGRAPH 2004*, volume 23, pages 303–308, 2004.

[57] D. Liu, Y. Xiong, L. Shapiro, and K. Pulli. Robust interactive image segmentation with automatic boundary refinement. In *IEEE International Conference on Image Processing*, 2010.

[58] J. Liu, J. Sun, and H.-Y. Shum. Paint selection. In *SIGGRAPH '09: ACM SIGGRAPH 2009 papers*, 2009.

[59] L. Liu and S. Sclaroff. Shape-guided split and merge of image regions. In *IWVF-4: Proceedings of the Fourth International Workshop on Visual Form*, pages 367–377. Springer-Verlag, 2001.

[60] N. Lu and X. Ke. A segmentation method based on gray-scale morphological filter and watershed algorithm for touching objects image. In *International Conference on Fuzzy Systems and Knowledge Delivery*, pages 474–478, 2007.

[61] J. Malcolm, Y. Rathi, and A. Tannenbaum. Graph cut segmentation with nonlinear shape priors. In *Proceedings of the Fourteenth IEEE International Conference on Image Processing*, volume 4, pages 365–368, 2007.

[62] F. Meyer and S. Beucher. Morphological segmentation. *Journal of Visual Communication and Image Representation*, 1(1):21–46, 1990.

[63] E. N. Mortensen and W. A. Barrett. Intelligent scissors for image composition. In *Computer Graphics, SIGGRAPH Proceedings*, pages 191–198, 1995.

[64] E. N. Mortensen and W. A. Barrett. Interactive segmentation with intelligent scissors. In *Graphical Models and Image Processing*, volume 60, pages 349–384, 1998.

[65] D. P. Mukherjee, Y. Potapovich, I. Levner, and H. Zhang. Ore image segmentation by learning image and shape features. *Pattern Recognition Letters*, 30(6):615–622, April 2009.

[66] S. D. Olabarriaga. *Human-Computer Interaction for the Segmentation of Medical Images*. PhD thesis, University of Amsterdam, 1999.

[67] D. R. Olsen, Jr. and M. K. Harris. Edge-respecting brushes. In *Proceedings of the 21st annual ACM symposium on User interface software and technology*, pages 171–180, 2008.

[68] N. Otsu. A threshold selection method from gray-level histogram. *IEEE Transaction on Systems Man. Cyber*, pages 62–66, 1979.

[69] B. Peng and O. Veksler. Parameter selection for graph cut based image segmentation. In *British Machine Vision Conference*, 2008.

[70] M. Polak, H. Zhang, and M. Pi. An evaluation metric for image segmentation of multiple objects. *Image and Vision Computing*, 27(8):1223–1227, July 2009.

[71] C. Rother, V. Kolmogorov, and A. Blake. GrabCut: Interactive foreground extraction using iterated graph cuts. *ACM Transactions on Graphics*, 23:309–314, 2004.

[72] C. D. Ruberto, A. Dempster, S. Khan, and B. Jarra. Segmentation of blood images using morphological operators. In *International Conference on Pattern Recognition*, pages 397–400, 2000.

[73] B. N. Saha. *The Evolution of Snake toward Automation for Multiple Blob-Object Segmentation*. PhD thesis, Department of Computing Science, University of Alberta, 2011.

[74] B. N. Saha, N. Ray, and H. Zhang. Snake validation: A PCA-based outlier detection method. *IEEE Signal Processing Letters*, 16(6):549–552, June 2009.

[75] E. Sarigul. *Interactive Machine Learning for Refinement and Analysis of Segmented CT/MRI Images*. PhD thesis, Virginia Polytechnic Institute and State University, September 2004.

[76] J. Shi. Adaptive local threshold with shape information and its application to oil sand image segmentation. Master's Thesis, University of Alberta, 2010.

[77] J. Shi, H. Zhang, and N. Ray. Solidity based local threshold for oil sand image segmentation. In *16th IEEE International Conference on Image Processing*, pages 2385–2388, November 2009.

[78] M. Singh, G. D. Seyranian, and D. D. Hoffman. Parsing silhouettes: The short-cut rule. *Perception and Psychophysics*, 61:636–660, 1999.

[79] G. Slabaugh and G. Unal. Graph cuts segmentation using an elliptical shape prior. In *International Conference on Image Processing*, volume 2, 2005.

[80] Z. Song, N. Tustison, B. Avants, and J. Gee. Adaptive graph cuts with tissue priors for brain MRI segmentation. In *IEEE International Symposium on Biomedical Imaging*, 2006.

[81] M. B. Stegmann and D. D. Gomez. A brief introduction to statistical shape analysis, March 2002.

[82] D. Stoyan and H. Stoyan. *Fractals, Random Shapes and Point Fields: Methods of Geometrical Statistics*. John Wiley & Sons, Chichester, September 1994.

[83] N. Sweeney and B. Sweeney. Efficient segmentation of cellular images using gradient-based methods and simple morphological filters. In *Engineering in Medicine and Biology Society*, pages 880–882, 1997.

[84] O. Veksler. *Efficient Graph-based Energy Minimization Methods in Computer Vision*. PhD thesis, Cornell University, 1999.

[85] O. Veskler. Star shape prior for graph-cut image segmentation. In *IEEE European Conference on Computer Vision*, pages 454–467, 2008.

[86] N. Vu and B. Manjunath. Shape prior segmentation of multiple objects with graph cuts. In *IEEE Conference on Computer Vision and Pattern Recognition*, pages 1–8, 2008.

[87] H. Wang and H. Zhang. Adaptive shape prior in graph cut segmentation. In *IEEE International Conference on Image Processing*, September 2010.

[88] H. Wang and H. Zhang. Improving image segmentation via shape PCA reconstruction. In *IEEE International Conference on Acoustics, Speech and Signal Processing*, March 2010.

[89] H. Wang, H. Zhang, and N. Ray. Clump splitting via bottleneck detection and shape classification. *Pattern Recognition*, January 2012.

[90] J. Wang, M. Agrawala, and M. F. Cohen. Soft scissors: an interactive tool for realtime high quality matting. In *SIGGRAPH '07: ACM SIGGRAPH 2007 papers*, New York, NY, USA, 2007. ACM.

[91] W. Wang and H. Sung. Cell cluster image segmentation on form analysis. In *International Conference of Natural Computation*, pages 833–836, 2007.

[92] W. X. Wang. Binary image segmentation of aggregates based on polygonal approximation and classification of concavities. *Pattern Recognition*, 31(10):1503–1524, 1998.

[93] Y. Wang and L. H. Staib. Boundary finding with correspondence using statistical shape models. In *IEEE Conference on Computer Vision and Pattern Recognition*, pages 338–345, 1998.

[94] T. P. Weldon. Removal of image segmentation boundary errors using an N-ary morphological operator. In *SoutheastCon, 2007*, pages 509–513, 2007.

[95] Q. Wen, H. Chang, and B. Parvin. A delaunay triangulation approach for segmenting clumps of nuclei. In *IEEE International Symposium on Biomedical Imaging*, pages 9–12, 2009.

[96] Q. Yang, C. Wang, X. Tang, M. Chen, and Z. Ye. Progressive cut: an image cutout algorithm that models user intentions. *IEEE Multimedia*, 14(3):55–66, 2007.

[97] T. T. E. Yeo, X. C. Jin, S. H. H. Ong, and R. S. Jayasooriah. Clump splitting through concavity analysis. *Pattern Recognition Letters*, 15(10):1013–1018, October 1994.

[98] A. Zadorozny. Contrast enhancement of oil sand images using morphological scale space. Master's Thesis, University of Alberta, 2006.

[99] D. Zhang and G. Lu. Review of shape representation and description techniques. *Pattern Recognition*, 37:1–19, 2004.

[100] H. Zhang. Image processing for the oil sands mining industry. *IEEE Signal Processing Magazine*, 25:198–200, November 2008.

[101] J. Zhu-Jacquot. Graph cuts segmentation with geometric shape priors for medical images. In *Proceedings of the 2008 IEEE Southwest Symposium on Image Analysis and Interpretation*, pages 109–112, Washington, DC, USA, 2008. IEEE Computer Society.